Cell

Article

Unraveling the Biology of a Fungal Meningitis Pathogen Using Chemical Genetics

Jessica C.S. Brown,[1,6] Justin Nelson,[2] Benjamin VanderSluis,[2] Raamesh Deshpande,[2] Arielle Butts,[3] Sarah Kagan,[4] Itzhack Polacheck,[4] Damian J. Krysan,[3,5] Chad L. Myers,[2,*] and Hiten D. Madhani[1,*]

[1]Department of Biochemistry and Biophysics, University of California, San Francisco, San Francisco, CA 94158, USA
[2]Department of Computer Science and Engineering, University of Minnesota, Minneapolis, MN 55455, USA
[3]Department of Chemistry, University of Rochester Medical Center, Rochester, NY 14643, USA
[4]Department of Clinical Microbiology and Infection Diseases, Hadassah-Hebrew University Medical Center, Jerusalem 91120, Israel
[5]Departments of Pediatrics and Microbiology/Immunology, University of Rochester School of Medicine and Dentistry, Rochester, NY 14643, USA
[6]Present address: Department of Pathology, Division of Microbiology and Immunology, University of Utah School of Medicine, Salt Lake City, UT 84112, USA
*Correspondence: cmyers@cs.umn.edu (C.L.M.), hitenmadhani@gmail.com (H.D.M.)
http://dx.doi.org/10.1016/j.cell.2014.10.044

SUMMARY

The fungal meningitis pathogen *Cryptococcus neoformans* is a central driver of mortality in HIV/AIDS. We report a genome-scale chemical genetic data map for this pathogen that quantifies the impact of 439 small-molecule challenges on 1,448 gene knockouts. We identified chemical phenotypes for 83% of mutants screened and at least one genetic response for each compound. *C. neoformans* chemical-genetic responses are largely distinct from orthologous published profiles of *Saccharomyces cerevisiae*, demonstrating the importance of pathogen-centered studies. We used the chemical-genetic matrix to predict novel pathogenicity genes, infer compound mode of action, and to develop an algorithm, O2M, that predicts antifungal synergies. These predictions were experimentally validated, thereby identifying virulence genes, a molecule that triggers G2/M arrest and inhibits the Cdc25 phosphatase, and many compounds that synergize with the antifungal drug fluconazole. Our work establishes a chemical-genetic foundation for approaching an infection responsible for greater than one-third of AIDS-related deaths.

INTRODUCTION

Invasive fungal infections are notoriously difficult to diagnose and treat, resulting in high mortality rates, even with state-of-the art treatments. The three most common pathogenic agents are *Cryptococcus neoformans, Candida albicans*, and *Aspergillus fumigatus* (Mandell et al., 2010). These organisms are opportunistic fungi that prey on individuals with varying degrees of immune deficiency. Susceptible patient populations include premature infants, diabetics, individuals with liver disease, chemotherapy patients, organ transplant recipients, and those infected with HIV (Mandell et al., 2010). Compounding the clinical challenge is the slow pace of antifungal drug development: only a single new class of drugs (the echinocandins) has been approved for use in the United States in the last 30 years (Butts and Krysan, 2012; Mandell et al., 2010; Roemer et al., 2011).

Fungal infections are estimated to cause 50% of deaths related to AIDS and have been termed a "neglected epidemic" (Armstrong-James et al., 2014). The fungus chiefly responsible for deaths in this population is *C. neoformans* (Armstrong-James et al., 2014). *C. neoformans* is an encapsulated basidiomycetous haploid yeast distantly related to *Saccharomyces cerevisiae* and *Schizosaccharomyces pombe*. A 2009 CDC study estimated that ~1 million infections and ~600,000 deaths annually are caused by *C. neoformans*, exceeding the estimated worldwide death toll from breast cancer (Lozano et al., 2012; Park et al., 2009). *C. neoformans* is widespread in the environment and exposure occurs through inhalation of desiccated yeast or spores (Heitman et al., 2011). In immunocompromised patients, *C. neoformans* replicates and disseminates, causing meningoencephalitis that is lethal without treatment (Heitman et al., 2011). Induction therapy involves flucytosine and intravenous infusions of amphotericin B (Loyse et al., 2013). Both drugs are highly toxic, difficult to administer, and neither is readily available in the areas with the highest rates of disease. The current recommendation for Cryptococcosis treatment is at least a year of therapy, which is difficult to accomplish in resource-limited settings (WHO, 2011). Thus, as is the case with infections caused by other fungal pathogens, effective treatment of cryptococcal infections is limited by the efficacy, toxicity, and availability of current pharmaceuticals.

We implemented chemogenomic profiling to approach the challenges of therapeutic development in *C. neoformans*. This method involves the systematic measurement of the impact of compounds on the growth of defined null mutants to produce a chemical-genetic map. Such a map represents a quantitative description composed of numerical scores indicative of the growth behavior of each knockout mutant under each chemical condition. Cluster analysis of the growth scores for large

numbers of mutants under many chemical conditions can reveal genes that function in the same pathway and even those whose products are part of the same protein complex (Collins et al., 2007; Parsons et al., 2004; Parsons et al., 2006). In addition, the identity of genes whose mutation produce resistance or sensitivity is useful for uncovering compound mode of action (MOA) (Hillenmeyer et al., 2008; Jiang et al., 2008; Nichols et al., 2011; Parsons et al., 2006; Xu et al., 2007; Xu et al., 2009). Large-scale studies have been restricted to model organisms for which gene deletion collections have been constructed, namely *S. cerevisiae*, *S. pombe*, and *Escherichia coli* K12 (Hillenmeyer et al., 2008; Nichols et al., 2011; Parsons et al., 2006). However, as none of these are pathogens, the extent to which the resulting insights translate to pathogenic organisms is unknown. A variation on chemogenomic profiling, chemically-induced haploinsufficiency, was first developed using a diploid heterozygote gene deletion library *S. cerevisiae* to identify compound MOA. This method, which identifies genes that impact compound sensitivity based on a two-fold gene dosage change, is suited for diploid organisms and has been used in the pathogen *C. albicans* (Jiang et al., 2008; Xu et al., 2007; Xu et al., 2009).

We report here the generation of a large-scale chemogenomic map for *C. neoformans* using defined, commonly available knockout mutants, assessments of data quality, and extensive experimental verification. Comparisons of the *C. neoformans* profile with two large-scale published profiles from *S. cerevisiae* revealed that for most types of compounds, the chemical-genetic interactions are distinct even among orthologous genes, emphasizing the importance of pathogen-focused investigation. We used nearest-neighbor analysis to predict new genes involved in polysaccharide capsule formation and infectivity, which we validated through experiment. We also utilized genetic responses to predict the G2/M phase of the cell cycle and the Cdc25 phosphatase as targets of a thiazolidone-2,4-dione derivative, which we confirmed in vivo and in vitro. Finally, because of the unmet need for improved antifungal drug efficacy, we developed a new algorithm, O2M, to predict new compound synergies based on the profiles of pairs known to be synergistic. Experimental tests demonstrate that the method performs vastly better than random expectation, thereby enabling the identification of synergistic compound combinations. Our studies establish a chemical-genetic foundation to approach the biology and treatments of *C. neoformans* infections, which are responsible for more than one-third of HIV/AIDS deaths worldwide.

RESULTS

A Chemical-Genetic Map of *C. neoformans*

We assembled 1,448 *C. neoformans* gene deletion strains (Chun et al., 2011; Liu et al., 2008) (Table S1 available online), corresponding to a substantial fraction of 6,967 predicted *C. neoformans* genes (Janbon et al., 2014), and a collection of compounds for screening (Table 1). Compounds were selected based on cost and literature evidence that they could inhibit the growth of fungi. Where feasible, compounds were chosen that are known to target specific biological processes. For each small molecule, we determined an approximate minimum inhibitory concentration (MIC) in agar, then measured growth of the knockout collection on each small molecule at 50%, 25%, and 12.5% MIC using high density agar plate colony arrays and a robotic replicator. We then measured the size of each colony using flatbed scanning and colony measurement software (Dittmar et al., 2010). We performed a minimum of four replicate colony measurements for each mutant-condition pair. Plate-based assays are subject to known nonbiological effects, such as spatial patterns. To mitigate these errors, a series of corrective measures were implemented using approaches described previously, including manual filtration of noisy data, spatial effect normalization and machine learning-based batch correction (Baryshnikova et al., 2010). In addition, the data for each deletion mutant and compound was centered and normalized. Each mutant-small molecule combination was assigned a score with positive scores representing relative resistance and negative scores representing compound sensitivity (Table S2). A global summary of the processed data organized by hierarchical clustering is shown in Figure 1A.

The importance and validity of the computational corrections is shown in Figures 1B and S1. We estimated how reproducible the chemical-genetic profiles were by calculating the correlation scores for data obtained for different concentrations of the same small molecule (purple). This measures the degree of overlap between the overall chemical-genetic profiles, which are themselves each composed of a score for each mutant-small molecule combination. We found significant correlation ($p = 2.67 \times 10^{-176}$) between data obtained for different concentrations of the same small molecule compared to those between profiles generated by data set randomization, suggesting significant reproducibility. Moreover, correlation scores between chemical-genetic profiles of different concentrations of different compounds (gray) are centered at approximately 0 (Figure 1B). This difference in correlation scores is apparent even when comparing experiments performed on the same day, when spurious batch signal can contribute to false positives (Baryshnikova et al., 2010). Our batch-correction algorithms resulted in same-batch screening data with strong positive correlation scores for the same compounds but correlation scores close to zero for different compounds (Figure S1), demonstrating successful removal of spurious signal (Baryshnikova et al., 2010). We compared chemical-genetic profiles between compounds in the azole family (Figure 1C). Despite the fact that the azoles tested include those of diverse uses, from agricultural pesticides to FDA-approved drugs (Table 1), many exhibit a significant profile correlation ($p = 2.82 \times 10^{-6}$), further indicating significant signal in the data. As a final assessment, we performed hypergeometric testing across all compounds to determine whether the same sensitive gene knockouts (defined by $Z < -2.5$) are identified at different concentrations of the same compounds. Using a Bonferonni-corrected p value cutoff, nearly all compounds display significant overlap of responsive genes at different concentrations (Figure 1D).

We assigned at least one phenotype (sensitivity or resistance to a compound) to 1,198 of 1,448 mutants (Figure 1E, Tables S2, S3, and S4). Of these, 855 exhibit one to ten phenotypes, while remaining 343 displayed from 11 to 146 phenotypes. Gene

Table 1. Small Molecules and Targets

Inhibitor (Activator)	Highest Screening Conc.	Process/Enzyme	Category	Pubchem ID	FDA Approval?
1-10 phenanthroline hydrochloride monohydrate	2 uM	broad/transition metal complexes	broad spectrum	2723715	no
2-aminobenzothiazole	30 uM	cytoskeleton function/ kinesin Kip1	cell structure	8706	no
2-hydroxyethylhydrazine	0.156%	lipid synthesis/phospholipid methylation	lipid biosynthesis	8017	no
3-aminotriazole	6.25 mM	histidine synthesis/IMP dehydratase	metabolism	1639	no
4-hydroxytamoxifen	1.56 uM	estrogen receptor (mammals)	signaling	449459	yes
5-fluorocytosine	2.5 ug/ml	DNA/RNA biosynthesis	DNA homeostasis/ protein synthesis	3366	yes
5-methyltryptophan	8 mM	tryptophan synthesis	metabolism	150990	no
Abietic acid	1 mM	lipid synthesis/lipoxygenase	lipid biosynthesis	10569	no
Acifluorfen methyl	156.25 ng/ml	porphyrin synthesis/ protoporphyrinogen oxidase	metabolism	91642	no
(Aconitine)	200 ug/ml	membrane potential/Na^+ channels (mammals)	membrane polarization	245005	no
Aflatoxin B1	100 ug/ml	DNA damaging agent	DNA homeostasis	14403	no
Agelasine D	5 ug/ml	membrane potential/Na^+/ K+-ATPase (mammals)	membrane polarization	46231918	no
Alamethicin/U-22324	60 uM	membrane integrity/forms a voltage-depended ion channel	membrane polarization	16132042	no
Alexidine dihydrochloride	125 ug/ml	antimicrobial/mitochondria	mitochondria	102678	yes
Allantoin	100 ug/ml	nitrogen-rich compound	metabolism	204	topical
Alternariol	2.5 ug/ml	cholinesterase inhibitor/sodium channel activator and DNA supercoiling/topoisomerase I	broad spectrum	5359485	no
Alumininum sulfate	1.5625 mM	unknown	unknown	24850	no
(Amantadine hydrochloride)	1.25 mM	neurotransmitter release/ glutamate receptor	signaling	64150	yes
Amiodarone	60 ug/ml	membrane potential/Na^+/ K+-ATPase (mammals)	membrane polarization	2157	yes
(Ammonium persulfate)	50 mM	reactive oxygen species	apoptosis/stress response/ damage response	62648	no
Amphotericin B	1 ug/ml	lipid biosynthesis/ergosterol	membrane integrity	5280965	yes
Andrastin A	4 ug/ml	protein modification/ farnesyltransferase	protein trafficking	6712564	no
Anisomycin	50 uM	translation/peptidyl transferase	gene expression	253602	no
Antimycin	100 ug/ml	respiration/cytochrome B	metabolism	14957	no
Apicidin	312.5 ng/ml	chromatin regulation/HDACs	gene expression	6918328	no
Artemisinin	312.5 mM	iron metabolism/hematin detoxification	metabolism	68827	yes
Ascomycin	3.125 uM	signaling/calcineurin	signaling	6437370	yes
Azide	62.5 uM	respiration/cytochrome C oxidase	metabolism	33558	no
Barium chloride	16 mM	metal homeostasis/diverse	broad spectrum/unknown	25204	no
Bafilomycin	4 ug/ml	autophagy/vacuolar-type H^+-ATPase	protein turnover	6436223	no
Bathocuproine disulphonic acid (BCS)	3 mM	copper acquisition	metabolism	16211287	no

(*Continued on next page*)

Table 1. *Continued*

Inhibitor (Activator)	Highest Screening Conc.	Process/Enzyme	Category	Pubchem ID	FDA Approval?
Bathophenanthroline disulfonate (BPS)	300 uM	iron acquistion/Fet3-Ftr1	metabolism	65368	no
Benomyl	100 ug/ml	cytoskeleton function/tubulin	cell structure	28780	no
(Betulinic acid)	64 ug/ml	protein degradation/proteasome	protein turnover	64971	no
Bifonazole	50 ug/ml	lipid biosynthesis/HMG-CoA and ergosterol biosynthesis	membrane integrity	2378	no
Brefeldin A	40 ug/ml	ER-Golgi Transport/ARF GEF	secretion	5287620	no
Calcium chloride	16 mM	metal homeostasis/diverse	broad spectrum	5284359	no
Caffeine	2.5 mM	DNA damage checkpoint/ATM	DNA homeostasis	2519	no
Calcium ionophore A23187	2.5 ug/ml	membrane integrity/peptide that acts as ionophore	membrane integrity	40486	no
Calcofluor white	500 ug/ml	cell wall synthesis/chitin and cellulose	cell wall	6108780	no
Camptothecin	500 ug/ml	DNA supercoiling/topoisomerase I	DNA homeostasis	24360	analog
Castanospermine	2.4 mM	protein modification/glycosidation	protein modification	54445	derivative
Cadmium chloride	1 mM	metal homeostasis/diverse	broad spectrum/unknown	24947	no
Cerulenin	312.5 ng/ml	fatty acid synthesis/beta-ketoacyl-acyl carrier protein synthase	lipid biosynthesis	5282054	no
Cesium chloride	128 mM	metal homeostasis/diverse	broad spectrum/unknown	24293	no
Chlorpromazine hydrochloride	1.5625 uM	phenothiazine antipsychotic drug (mammals)/dopamine, seratonin, and other neuroreceptors	signaling	6240	yes
Chromium (III) chloride	8 mM	metal homeostasis/diverse	broad spectrum	16211596	no
Ciclopirox olamine	750 ng/ml	iron acquisition and other	metabolism	38911	yes
Cisplatin	100 ug/ml	DNA synthesis	DNA homeostasis	157432	yes
Climbazole	0.03125%	lipid biosynthesis/ergosterol biosynthesis and respiration/ cytochrome P450	broad spectrum	37907	topical
Clotrimazole	500 nM	lipid biosynthesis/ergosterol biosynthesis	membrane integrity	2812	yes
Colistin	1 mg/ml	membrane integrity	membrane integrity	5311054	yes
Congo red	0.0625%	cell wall synthesis/chitin, cellulose, and glucan	cell wall	11313	no
Coniine	0.15625%	neurosignaling (mammals)/ nicotinic receptor	signaling	441072	no
(Crystal violet)	0.0012500%	oxidative stress inducer	stress response	11057	topical
CuCl2	8 mM	copper homeostasis/diverse	metabolism	24014	no
Cycloheximide	1.875 ug/ml	translation/ribosome	gene expression	6197	no
Cyclopiazonic acid	15.625 uM	ion transport and cell polarization (mammals)/Ca^{2+}- ATPase	metabolism	54682463	no
Cyclosporin	75 ug/ml	signaling/calcineurin	signaling	5284373	yes
Cyproconazole	1.5625 ug/ml	lipid biosynthesis/ergosterol biosynthesis	membrane integrity	86132	no
Cyprodinil	10 ug/ml	methionine biosynthesis	metabolism	86367	no
Daphnetin	100 uM	signaling/PKA, PKC, EGR receptor, others	signaling	5280569	no
Desipramine hydrochloride	250 uM	neurosignaling (mammals)/ norepinephrine transporter	signaling	65327	yes

(*Continued on next page*)

Table 1. *Continued*

Inhibitor (Activator)	Highest Screening Conc.	Process/Enzyme	Category	Pubchem ID	FDA Approval?
Dyclonine hydrochloride	3.125 uM	lipid biosynthesis/ergosterol biosynthesis	membrane integrity	68304	yes
Emetine dihydrochloride hydrate	5 mM	translation/ribosome	gene expression	3068143	yes
Emodin	62.5 uM	signaling/CK2, others	signaling	3220	yes
Erlotinib	50 ug/ml	signaling (mammals)/EGFR tyrosine kinase	signaling	176870	yes
FeCl3	32 mM	iron acquisition, metal homeostasis	metabolism	24380	no
Fenoxanil	80 ug/ml	melanin biosynthesis	metabolism	11262655	no
Fenpropimorph	2.5 ug/ml	sterol synthesis	lipid biosynthesis	93365	no
FK506	312.5 ng/ml	signaling/calcineurin	signaling	445643	yes
Fluconazole	10 ug/ml	lipid biosynthesis/ergosterol biosynthesis	membrane integrity	3365	yes
Fluspirilene	25 uM	antipsychotic drug, mechanism of action unknown	unknown	3396	yes
Gallium (III) nitrate	25 mM	metal homeostasis/diverse	broad spectrum	57352728	no
Geldanamycin	2 uM	protein folding/Hsp90	protein folding	5288382	trials
(H2O2)	6 mM	reactive oxygen species	apoptosis/ stress response/damage response	784	topical
Haloperidol	125 uM	phenothiazine antipsychotic drug (mammals)/dopamine, seratonin, and other neuroreceptors	signaling	3559	yes
Harmine hydrochloride	1 mM	cell differentiation (mammals)/ PPARgamma	signaling	5359389	yes
Hydroxyurea	12.5 mM	DNA replication/replication fork progression	DNA homeostasis	3657	yes
Hygromycin	37.5 ug/ml	translation/ribosome	gene expression	35766	no
Imazalil	25 ug/ml	lipid biosynthesis/ergosterol synthesis	membrane integrity	37175	no
Iodoacetate	500 uM	protein degradation/cysteine peptidases	protein turnover	5240	no
Itraconazole	1.5625 ug/ml	lipid biosynthesis/ergosterol synthesis	membrane integrity	55283	yes
K252a	10 ug/ml	signaling/variety of kinases	signaling	127357	trials
Latrunculin	25 uM	cytoskeleton function/actin	cell structure	445420	no
Lead (II) nitrate	64 mM	metal homeostasis/diverse	broad spectrum	24924	no
Leptomycin	1.25 ug/ml	nucleocytoplasmic transport/ Crm1	gene expression	6917907	no
LiCl	37.5 mM	metal homeostasis/diverse	broad spectrum/ unknown	433294	no
Lovastatin	37.5 ug/ml	sterol synthesis/HMG CoA reductase	metabolism	53232	yes
LY 294002	375 uM	signaling/PI3K	signaling	3973	no
Magnesium chloride	150 mM	metal homeostasis/diverse	broad spectrum	21225507	no
Malachite green	3.125 ug/ml	antimicrobial/unknown	antimicrobial	11294	no
Manganese sulfate	128 mM	metal homeostasis/diverse	metabolism	177577	no
Mastoparan	5 uM	signaling/G-proteins	signaling	5464497	no
(Menadione)	150 uM	vitamin K3/reactive oxygen species	diverse	4055	yes

(*Continued on next page*)

Table 1. *Continued*

Inhibitor (Activator)	Highest Screening Conc.	Process/Enzyme	Category	Pubchem ID	FDA Approval?
Menthol	1 mM	voltage-dependent ion channels (mammals)/sodium channel	signaling	16666	yes
Methotrexate	2.5 uM	folate synthesis/DHFR	metabolism	126941	yes
Methyl methanesulfonate (MMS)	0.0165%	DNA replication/replication fork progression	DNA homeostasis	4156	no
Methylbenzethonium chloride (MBT)	0.25%	antimicrobial	antimicrobial	5702238	topical
MG132	12.5 uM	protein degradation/proteasome	protein turnover	462382	no
Miconazole	6.25 ug/ml	lipid biosynthesis/ergosterol synthesis	membrane integrity	4189	yes
Mitomycin C	12 uM	DNA damaging agent	DNA homeostasis	5746	yes
Myclobutanil	2 ug/ml	lipid biosynthesis/ergosterol synthesis	membrane integrity	6336	no
Mycophenolic acid	2.5 ug/ml	GMP synthesis/IMP dehydrogenase	metabolism	446541	yes
Myriocin	12.5 ug/ml	sphingolipid synthesis	metabolism	6438394	analog
NA8		unknown	unknown		no
(NaCl)	37.5 mM	osmotic regulation/HOG pathway	stress response	5234	yes
(NaNO2)	150 uM	reactive nitrogen species	stress response	23668193	no
Neomycin sulfate	2.4 mM	protein synthesis/ribosome	gene expression	8378	yes
Nicotinamide	25 uM	chromatin regulation/sirtuins	gene expression	936	yes
Nigericin	100 ug/ml	membrane integrity/ion gradient	membrane polarization	34230	no
Nikkomycin	5 ug/ml	chitin synthesis	cell wall	72479	trials
NiSO4	1 mM	antifungal/diverse	antifungal	5284429	no
Nocodazole	30 uM	cytoskeleton function/tubulin	cell structure	4122	no
Ophiobolin A	62.5 ng/ml	signaling/calmodulin	signaling	5281387	no
Parthenolide	150 uM	immune and inflammatory response/NF-kB	signaling	6473881	no
Pentamidine isethionate	500 uM	antimicrobial/mitochondrial function	antimicrobial	8813	yes
pH	8.0, 8.5, 9.0	pH homeostasis	diverse		no
Phenylarsine oxide	2.5 uM	broad/XCXXCX protein phosphatases	broad spectrum	4778	no
Picoxystrobin	6.25 ug/ml	quinone outside inhibitor class/fungal cytochrome bcl	mitochondria	11285653	no
(Plumbagin)	2.8 uM	reactive oxygen species	stress response	10205	no
PMSF	10 mM	vacuolar proteolysis/ proteinase B	signaling	4784	no
Polyoxin B	200 ug/ml	chitin synthesis	cell wall	3084093	no
Povidone iodine	2%	antimicrobial	antimicrobial	410087	topical
Prussian blue	75 mM	monocation chelator	metabolism	16211064	yes
Quinic acid	2 mM	antimicrobial	antimicrobial	6508	no
Rapamycin	0.125 uM	signaling/TOR kinases	signaling	5284616	yes
Rubidium chloride	150 mM	potassium metabolism/ competitor	metabolism	62683	no
Rifamycin SV monosodium salt	200 ug/ml	RNA synthesis/RNA polymerase	gene expression	6324616	yes
S10		unknown	unknown		no
S8		unknown	unknown		no

(*Continued on next page*)

Table 1. *Continued*

Inhibitor (Activator)	Highest Screening Conc.	Process/Enzyme	Category	Pubchem ID	FDA Approval?
S-aminoethyl-L-cysteine (thialysine)	10 uM	amino acid metabolism/lysine analog	metabolism	20048	no
SDS	0.0015625%	cell membrane integrity	membrane integrity	3423265	no
Selumetinib	150 ug/ml	signaling/MAPK (ERK)	signaling	10127622	trials
Sertraline	15 ug/ml	neurosignaling (mammals)/ seratonin reuptake	neurosignaling	68617	yes
Sodium azide	62.5 uM	respiration/cytochrome oxidase	mitochondria	33557	no
Sodium borate	10 mM	antimicrobial/diverse	antimicrobial	21749317	no
Sodium hydrosulfite	6.25 mM	antimicrobial, counteracts some antimicrobials	antimicrobial	24489	no
Sodium iodide	75 mM	antimicrobial	antimicrobial	5238	yes
Sodium metavanadate	10 mM	signaling/protein phosphotyrosine phosphatases	signaling	4148882	no
(Sodium molybdate)	64 mM	respiration/oxygen uptake	diverse	61424	no
Sodium selenite	4 mM	respiration/oxygen uptake	diverse	16210997	yes
Sodium sulfite	100 mM	ATP synthesis and accumulation/ unknown	metabolism	24437	no
Sodium tungstate	64 mM	metal homeostasis/diverse	broad spectrum/unknown	150191	no
Sorafenib	100 uM	signaling/VEGF tyrosine kinase	signaling	216239	yes
Staurosporine	3 uM	signaling/PKC1	signaling	5279	yes
(STF-62247)	400 uM	autophagy	protein turnover	704473	trials
Sulfometuron methyl	100 ug/ml	branch chain amino acid synthesis/acetolactate synthase	metabolism	52997	no
Suloctidil	400 uM	Ca^{2+} homeostasis in blood vessels (mammals)/putative Ca^{2+} channel blocker	vascular system/ metabolism	5354	formerly
Tamoxifen citrate	10 uM	estrogen signaling (mammals)/ estrogen receptor, mixed agonist/antagonist	signaling	2733525	yes
Taurolidine	0.01%	antimicrobial/lipopolysaccharide detection and signaling	host defense	29566	yes
Tautomycin	250 nM	signaling/PP2A	signaling	3034761	no
Tellurite	0.1%	sulfate assimilation	metabolism	115037	no
Terbinafine	75 uM	sterol synthesis/squalene epoxidase	metabolism	1549008	yes
Thiabendazole	200 ug/ml	respiration/NADH oxidase	mitochondria	5430	yes
Thonzonium bromide	25 uM	antimicrobial, pH homeostasis/ V-ATPase	broad spectrum	11102	yes
Tomatine	5 ug/ml	glycoalkaloid antifungal of unknown mechanism/ergosterol biosynthesis	antifungal/membrane integrity	28523	no
Trichostatin A	100 uM	chromatin regulation/HDACs	gene expression	444732	no
Trifluoperazine	200 uM	signaling/calmodulin	signaling	5566	yes
Trimethoprim	1.6 mg/ml	folate synthesis/DHFR	metabolism	5578	yes
Tunicamycin	2.5 ug/ml	glycosylation/Alg7	secretion	11104835	no
Usnic acid	25 ug/ml	antimicrobial	antimicrobial	6433557	trials
Valinomycin	20 uM	membrane integrity/potassium exclusion	membrane polarization	5649	no
Verrucarin	5 uM	protein biosynthesis/polysome	protein turnover	6437060	no
ZnCl2	4 mM	metal homeostasis/diverse	diverse	5727	no

A list of compounds used in this study, their targets, and the screening concentration.

deletions with the greatest number of phenotypes are *cnag_07622*Δ (encoding the COP9 signalosome subunit 1) and *cnag_05748*Δ (encoding a Nto1 subunit of the NuA3 histone acetyltransferase). Compounds that elicit the greatest number of responsive gene deletions (Figure 1F) are the heavy metal salt sodium tungstate and the trichothecene protein synthesis inhibitor verrucarin (Table S5), presumably reflecting the pleiotropic impact of these molecules on cells.

Gene Ontology Analysis Reveals Processes Associated with Drug Sensitivity

Drug influx and efflux is thought to be a major general determinant of microbial drug susceptibility (Fernández and Hancock, 2012), but we also sought functions involved in drug sensitivity. We investigated this question in an unbiased fashion by analyzing chemogenomic profiles using Gene Ontology (GO), a gene annotation approach useful for comparative analyses. We first identified annotated orthologs of *C. neoformans* genes represented in the deletion library and associated GO terms with these orthologs. We then determined whether the sensitive gene knockouts that respond to each small molecule are enriched for association with particular GO terms relative to a randomized control set (Figure 2, Table S6). We observed that protein transport-related terms are highly enriched, as are processes related to ubiquitin modification/proteolysis and vesicle-mediated transport. These terms are associated with nine and five compounds, respectively, suggesting that intracellular transport and ubiquitin-mediated protein turnover may play important general roles in drug sensitivity.

Comparison with *S. cerevisiae* Chemogenomic Profiling Data Sets

Chemogenomic profiling has been performed extensively in *S. cerevisiae*, allowing us to ask whether genetic responses to compounds were conserved. We performed a three-way comparison with two large-scale studies (Hillenmeyer et al., 2008; Parsons et al., 2006) (Figure 3A). Our data set has 46 compounds in common with Parsons et al. (2006) and 29 with Hillenmeyer et al. (2008); the two *S. cerevisiae* data sets had 15 compounds in common. First we identified genes whose knockouts exhibited a significant ($Z \leq -2.5$ or $\geq +2.5$) score (“responding”) when treated with a small molecule used in more than one data set, then identified which of those genes had orthologs in both *S. cerevisiae* and *C. neoformans*. We then calculated how many orthologs responded in both data sets. To adjust for a greater starting number of common genes when comparing the *S. cerevisiae* data sets to each other and control for functional biases, we limited this comparison to genes that also have orthologs in the *C. neoformans* knockout collection. The blue labels for compounds in Figures 3B–3D indicate statistically significant similarities ($p \leq 0.05$) in drug responses. Nearly all of the compounds in common between the two *S. cerevisiae* studies display statistically significant overlap in the genes that produced sensitivity to a given compound, despite the very different experimental platforms that were used to assess drug sensitivity/resistance (13/15 cases; Figure 3B). In striking contrast, few compounds show significantly conserved genetic responses when comparing either *S. cerevisiae* data set with the *C. neoformans* data. For the two *C. neoformans*-*S. cerevisiae* comparisons, only two of 46 compounds (Figure 3C) and one of 29 compounds (Figure 3D) show conserved responses, respectively.

The responses to azole compounds exhibit limited response conservation between species. Comparing our data set with Parsons et al., the responses to fluconazole (FLC) and clotrimazole, the azoles in both data sets, do not show significant overlap (Figure 3C). Likewise, between our data set and Hillenmeyer et al. (2008), no gene orthologs respond to miconazole and clotrimazole in both data sets (Figure 3D). In contrast, between the two *S. cerevisiae* data sets, the only shared azole, clotrimazole, shows a significantly similar response (Figure 3B). We compared published work that examined the transcriptome responses of *S. cerevisiae* (Kuo et al., 2010) and *C. neoformans* (Florio et al., 2011) to FLC. We found that, while there was significant overlap in orthologous genes impacted in the two species, ($p = 1.6 \times 10^{-3}$), there were also considerable differences: 67% of the genes with an altered response in *C. neoformans* whose orthologs in *S. cerevisiae* did not exhibit significant change, (Table S7) (Kuo et al., 2010).

Using Chemical-Genetic Signatures to Identify Capsule Biosynthesis Mutants

Studies in *S. cerevisiae* have shown that that the phenotypic signatures of gene deletions for genes that act in the same process or protein complex tend to be similar (Collins et al., 2007; Costanzo et al., 2010; Nichols et al., 2011; Parsons et al., 2004; Parsons et al., 2006). We reasoned that this property of could be used in a pathogen to identify candidates for new genes involved in virulence by simply testing gene deletions that displayed phenotypic profiles similar to those corresponding to known virulence factors.

C. neoformans harbors an inducible polysaccharide capsule that is unusual among fungi (Del Poeta, 2004; Doering, 2009; Haynes et al., 2011; Kumar et al., 2011; O’Meara and Alspaugh, 2012; O’Meara et al., 2010; Vecchiarelli et al., 2013). The principal polysaccharide component, glucuronylxylomannan (GXM), consists of a repeating glycan unit that has α-1,3-linked mannose backbone with side chains of β-linked glucuronic acid and xylose (Kozel et al., 2003). Capsule production is critical for virulence and the ability of *C. neoformans* to evade detection and destruction by the host immune system (Vecchiarelli et al., 2013).

To identify candidates for genes involved in capsule formation and/or attachment, we organized our data set using hierarchical clustering of growth phenotypes produced by compound exposure. We focused on two clusters, each containing a gene(s) previously implicated in capsule biosynthesis: *PBX1* and *CPL1* (Liu et al., 2008; Liu et al., 2007b) in one cluster (Figure 4A) and *CAP60* (Chang and Kwon-Chung, 1998) in a second cluster (Figure 4B). The *pbx1*Δ/*cpl1*Δ cluster contains nine genes and the *cap60*Δ cluster seven. We quantified capsule accumulation after induction by computing the ratio of the diameter of the cell and capsule to the diameter of the cell alone (Figures 4C and 4D). Wild-type cells exhibit high capsule production, *pbx1*Δ mutants display a partial defect (Liu et al., 2007a) and *cpl1*Δ and *cap60*Δ mutants are acapsular (Chang and Kwon-Chung, 1998; Liu et al.,

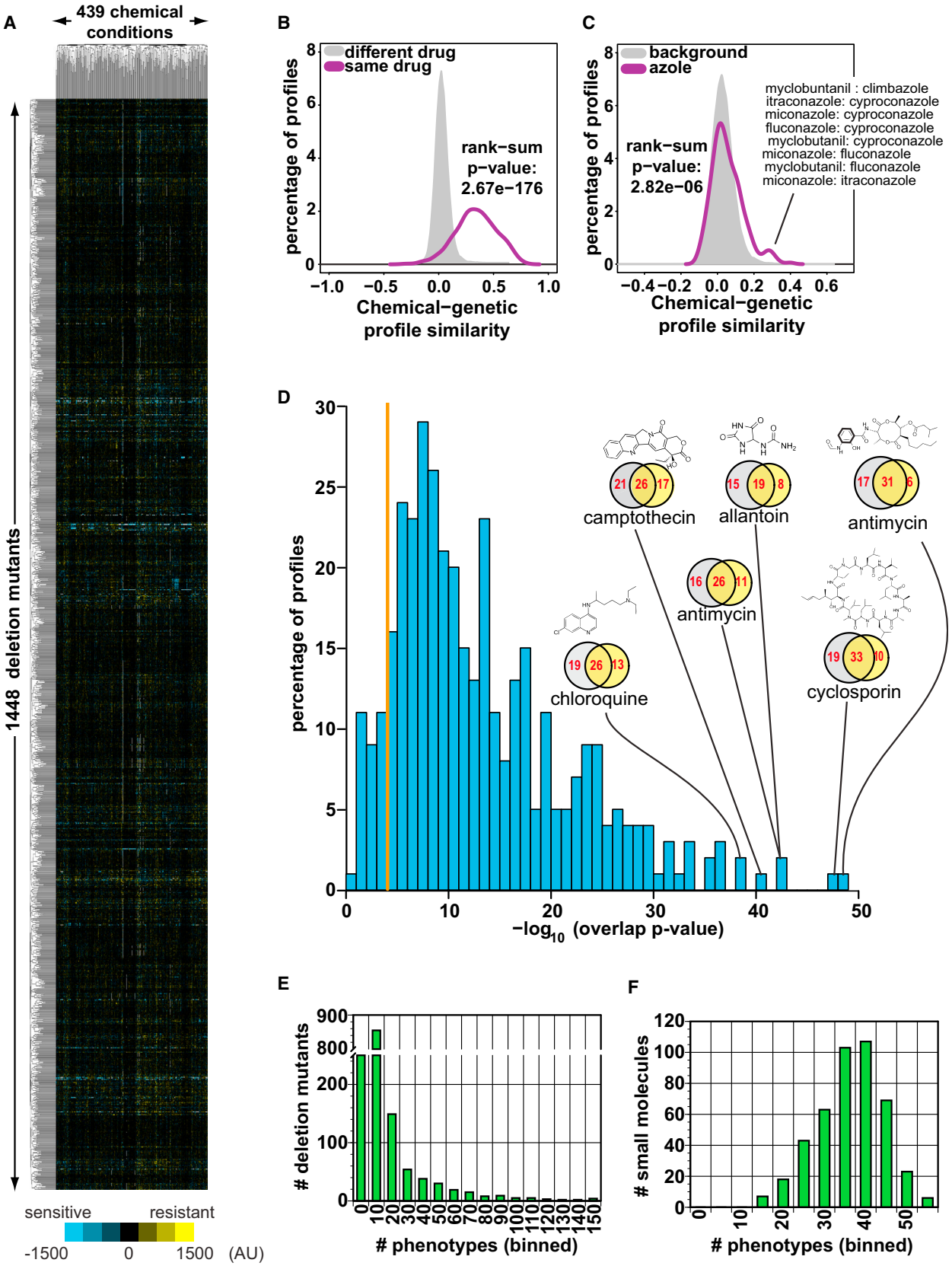

(legend on next page)

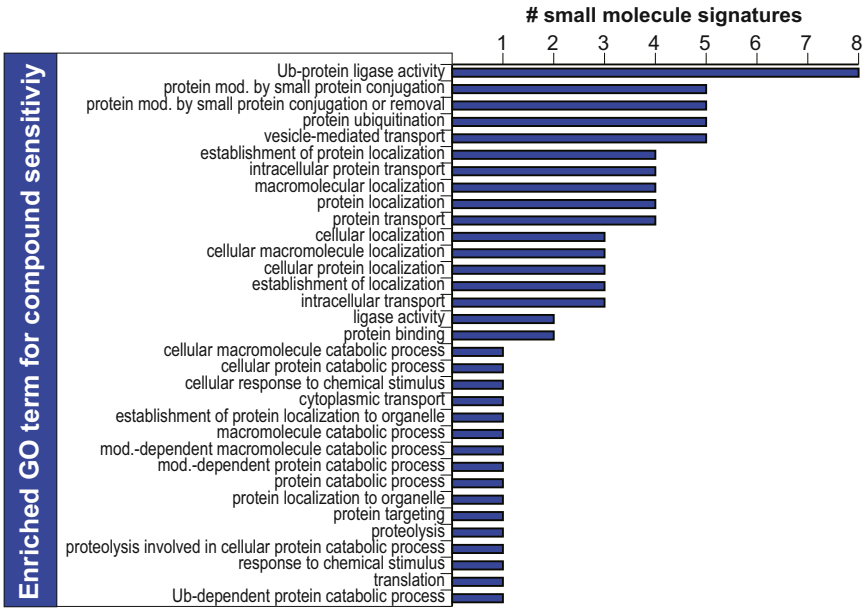

Figure 2. Determinants of Compound Sensitivity

We calculated whether molecules elicited a significant response from *C. neoformans* ORFs that are enriched for association with specific GO terms. Terms are listed on the y axis and the number of compounds whose responding gene knockouts associated with that GO term are listed on the x axis. See also Table S6.

2008). We found that seven of nine mutants in the *pbx1*Δ/*cpl1*Δ cluster exhibit a statistically significant capsule defect, as did four of the seven mutants in the *cap60*Δ cluster. In contrast, previous work from our laboratory found that approximately 1% of the original *C. neoformans* library shows a gross defect in capsule production (Liu et al., 2008).

Previous work showed that *pbx1*Δ mutants produce polysaccharide capsule whose attachment to the cell wall is sensitive to sonication, a finding that we confirmed (Figures 4C and 4D). We refer to the cell's ability to retain GXM on the cell surface as "capsule maintenance." Knockout mutants in *cnag_01058* do not exhibit a basal capsule defect but lost nearly 40% of their capsule diameter following sonication. Cells deleted for the *GCN5* gene, like *pbx1*Δ cells, show both decreased capsule levels and sonication-sensitive capsule. None of the mutants from the *cap60*Δ cluster produces a sonication-sensitive phenotype, suggesting that the *pbx1*Δ/*cpl1*Δ and *cap60*Δ clusters organize mutants that have distinct phenotypes. However, because several mutants do not produce visible capsule, the sonication test is insufficient to definitively measure capsule maintenance. We therefore analyzed how much glucoronoxylomannan (GXM), the major capsular polysaccharide (Doering, 2009), is secreted into the growth medium by blotting with α-GXM antibodies (Figure S2A). We found that two mutants that produce little (*gcn5*Δ) or no (*yap1*Δ) visible capsule still shed GXM into the medium, suggesting that they cannot retain capsule on their cell surface. Indeed, we found that they shed more GXM than *pbx1*Δ cells. Four of nine mutants in the *pbx1*Δ/*cpl1*Δ cluster exhibit a maintenance defect, whereas none of the *cap60*Δ cluster mutants do. We also found that GXM produced by these cells can be taken up and added to the surface ("donated") of an acapsular mutant using a standard GXM transfer assay (Kozel and Hermerath, 1984; Reese and Doering, 2003). Moreover, apparent capsule-defective mutants shed GXM (Figures S2B and S2C) and can donate GXM from conditioned medium (Figure S2C). Mutants that appear to not secrete GXM (*pbx1*Δ, *cpl1*Δ, and *sgf73*Δ) can donate it, but only if conditioned medium concentration is increased 10-fold (Figure S2D). These data are consistent with a recently published study on the role of Pbx1 in capsule attachment and assembly (Kumar et al., 2014).

Since the capsule is a major virulence trait of *C. neoformans*, we tested whether knockout mutants that exhibited a capsule defect displayed a defect in the mammalian host, using a murine inhalation model. We infected mice with a mixture of differentially-tagged wild-type and mutant cells at a ratio of 1:1. At 10 days

Figure 1. Chemical-Genetic Profiling of *C. neoformans*

(A) Heat map of full data set following hierarchical clustering. Compounds are arrayed on the x axis and gene knockouts on the y axis. See also Tables S1 and S2.

(B) Probability density function for pairwise correlation scores between the chemical genetic profiles of different compounds (gray) and the same compounds at different concentrations (purple) screened on different days (different batches).Scores between the chemical-genetic profiles of different concentrations of the same compounds are significantly higher than those between different compounds (Wilcoxon test, $p = 2.7 \times 10^{-176}$). See also Figure S1.

(C) Probability density function for pairwise correlation scores between the chemical genetic profiles of different compounds (gray) and azole family compounds (purple). Pairwise comparisons between azoles exhibit higher correlation scores than nonazole compounds (Wilcoxon test, $p = 2.8 \times 10^{-6}$). Molecules with the highest pairwise comparisons scores are listed on the right.

(D) Pearson's correlation score between two different concentrations of the same compounds. Concentrations with similar correlation scores are binned together (y axis). For compounds with the greatest correlation scores between concentrations, Venn diagrams of significant genes ($Z < -2.5$) present in profiles from the same compounds at different concentrations and the small-molecule structure are shown. The orange line indicates a hypergeometric p value ≤ 0.05

(E)Histogram showing the number of deletion mutants that have given number of phenotypes. A phenotype is considered $|Z| > 2.5$ and we identified phenotypes independently for each small-molecule concentration.

(F) Histogram showing the number of small molecules that have a given number of phenotypes. Phenotypes ($|Z| > 2.5$) were identified for each small-molecule condition/concentration

See also Figure S1 and Tables S1, S2, S3, S4, and S5.

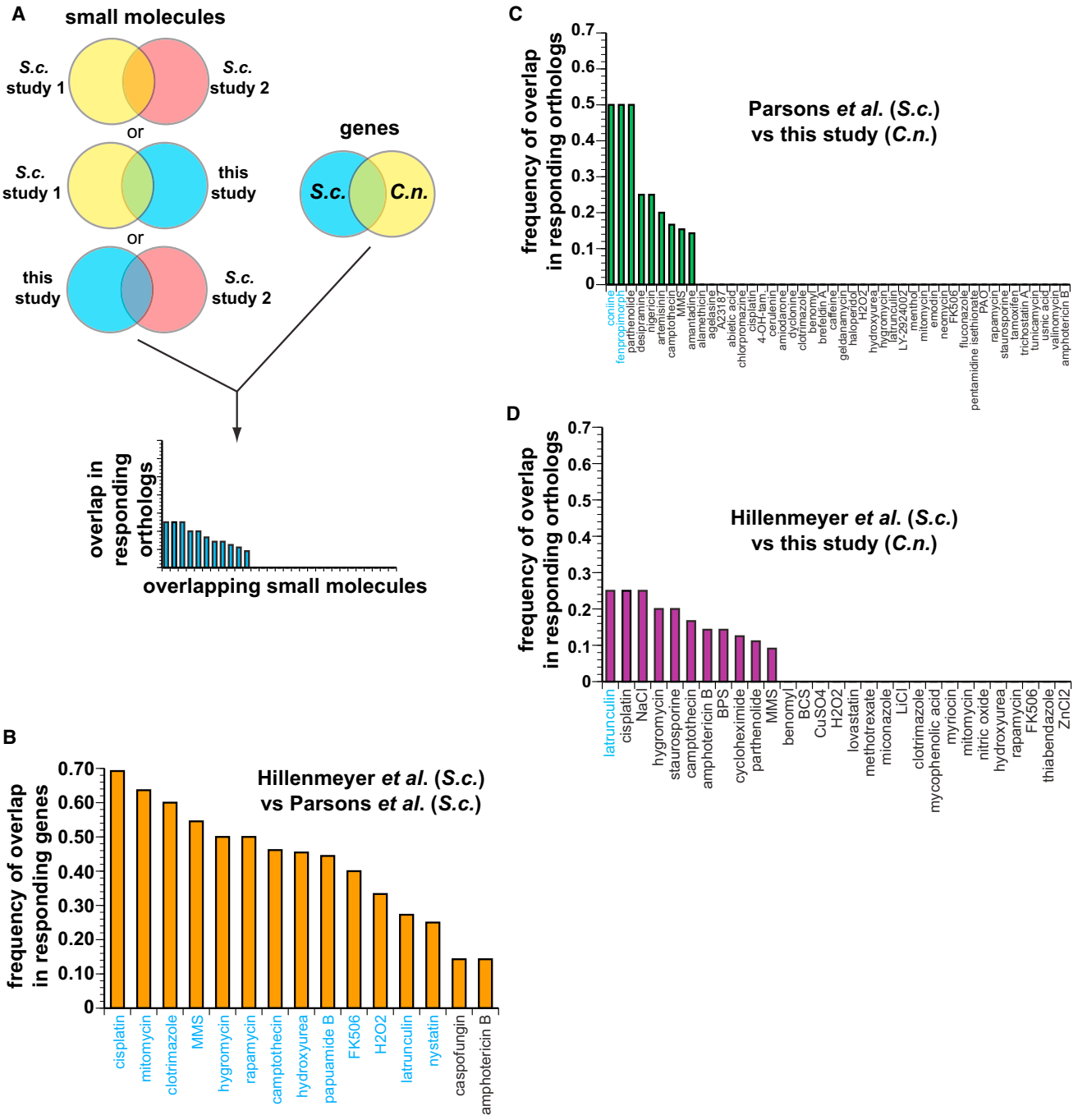

Figure 3. Chemical-Genetic Signatures of *C. neoformans* Genes Differ from Orthologous *S. cerevisiae* Genes

(A) Flowchart of computation process for comparing data sets. We identified *C. neoformans* and *S. cerevisiae* orthologous genes that were present in all data sets, then compared the responses of only those genes in all the data sets. We compared genes whose knockout mutants significantly ($|Z| > 2.5$) responded to compound that were common in at least two of the data sets.

(B) Comparison between Parsons et al. (2006) and Hillenmeyer et al. (2008), comparing the response ($|Z| > 2.5$) of genes that have orthologs present in the *C. neoformans* data set. Compounds whose profiles exhibit significant overlaps ($p < 0.05$) are labeled in blue.

(C) Comparison between our data set and Parsons et al. (2006) Compounds whose profiles exhibit significant overlaps ($p < 0.05$) are labeled in blue.

(D) Comparison between our data set and Hillenmeyer et al. (2008) Compounds whose profiles exhibit significant overlaps ($p < 0.05$) are labeled in blue.

postinfection (dpi), we sacrificed animals, harvested and homogenized lung tissue, then plated on the appropriate selective media for colony forming units (CFUs). All but one of the *pbx1*Δ/*cpl1*Δ cluster members were significantly underrepresented relative to wild-type; the exception was the *cnag_01058*Δ mutant, which is defective in capsule maintenance but not capsule biosynthesis (Figures 4C and S2A). *yap1*Δ cells, which appear acapsular but secrete GXM, displayed a major defect in fitness in the host (Figure 4E). Three of four *cap60*Δ cluster mutants also display a defect in accumulation of CFUs in host lungs (Figure 4E).

Chemogenomics Identifies the Cell Cycle as a Target of the Antifungal Small Molecule S8

We included a number of drug-like antifungal compounds in our screen in order to identify their targets (Table 1). Our use of *C. neoformans* chemogenomics to assist in the identification of a target of toremifene is described elsewhere (Butts et al., 2014). Here we investigate the thiazolidine-2,4-dione derivatives originally described for their activity against *C. albicans* biofilms (Kagan et al., 2014).

Our chemogenomic profiling data of the thiazolidine-2,4-dione derivative S8 revealed a striking outlier: a knockout mutant in the gene coding for a *C. neoformans* ortholog of the conserved cell-cycle kinase Wee1, is relatively resistant (Figure 5A). We observed resistance at multiple concentrations of S8 (Table S2). The related compound NA8, which contains a replacement of a sulfur atom with a carbon atom on the thiazolidinedione moiety (Figure 5B), does not elicit the same resistance (Figure S3A). The *wee1*Δ mutant is also resistant to S10 (Figure S3B), which harbors a C10 alkyl chain instead of C8 but is otherwise identical to S8 (Figure S3C).

Wee1 regulates the G2/M cell-cycle checkpoint through inhibitory phosphorylation of Cdk1, which in turn is required for cells to traverse the checkpoint. The essential phosphatase Cdc25 activates Cdk1 by removing the inhibitory phosphorylation added by Wee1 (Morgan, 2007) (Figure 5C). Because the *wee1*Δ is relatively resistant to S8, we hypothesized that S8 targeted a protein that acts through Wee1 to regulate Cdk1. One such target could be Cdc25.

We reasoned that if the Wee1/Cdc25-regulated step of the cell cycle were an important target of S8 in vivo, wild-type *C. neoformans* cells treated with S8 would arrest at G2/M. To test this prediction, we treated exponential cultures with S8, S10, or NA8 and examined the impact on the cell cycle. We harvested and fixed representative samples every 30 min, then analyzed DNA content by flow cytometry. Control cultures treated with DMSO (carrier) (Figure 5D) or the control compound NA8 (Figure 5E) stayed asynchronous for the entire 3.5 hr of the time course. Strikingly, S8-treated (Figure 5F) cells accumulated with 2C DNA content, which indicates G2/M arrest in *C. neoformans*, a haploid yeast (Whelan and Kwon-Chung, 1986). At later time points, cells synthesize DNA but do not complete mitosis and cytokinesis. This is consistent with observations in *S. pombe* that partial inhibition of Cdk1 permits re-replication of DNA (Broek et al., 1991).

Because inhibition of Cdc25 would provide a parsimonious explanation for the genetic and biological properties of S8, we tested whether S8 inhibits *C. neoformans* Cdc25 in vitro. We expressed and purified the catalytic domain of a *C. neoformans* ortholog (*CNAG_07942*) in *E. coli* (Figure S3D) and then performed in vitro phosphatase assays using 3-O-methyl fluorescein phosphate (OMFP) as a substrate (Figures 5G and 5H) (Hill et al., 1968). We observed that S8 inhibits Cdc25 activity (K_i ~140 μM, Figure 5E), as do both S10 (Figure S3E) and NSC 663284 (K_i~250 μM, Figure S3F), a commercially available inhibitor of mammalian Cdc25 (Pu et al., 2002). The control compound NA8 does not inhibit *C. neoformans* Cdc25 in vitro (Figure S3G). For S8, the in vitro inhibition constant is roughly comparable to the liquid MIC value against *C. neoformans*, which we measured to be ~60 μM in YNB. S10 has a higher K_i (K_i~310 μM) but similar to the MIC value (~55 μM) measured in YNB agar compared to S8.

O2M: A Genetic Biomarker Algorithm to Predict Compound Synergies

Drug resistance is a major clinical challenge in the treatment of both bacterial and fungal infections (Anderson, 2005; Cantas et al., 2013). An effective therapeutic strategy is to treat patients with drugs that act synergistically, enhancing each other's effectiveness beyond that produced by the sum of each drug's individual impact (Kalan and Wright, 2011). This approach is thought to decrease acquisition drug resistance, increase the available drug repertoire (Kalan and Wright, 2011) and ameliorate toxicities (Kathiravan et al., 2012; Lehár et al., 2009).

We hypothesized that we could use the chemogenomic information from our screens of drugs known to act synergistically, such as FLC and fenpropimorph (Jansen et al., 2009), to identify new synergistic interactions (Figure 6A). When we compared the identity of genes whose knockouts "responded" to each individual small molecule in a known synergistic pair ($|Z| \geq 2.5$, Tables S3 and S4), we found that this "responsive" gene set was significantly enriched over the expected value (Fisher's exact test, $p \leq 6 \times 10^{-5}$) (Figure 6A, top). This observation is consistent with a previous report that the chemical-genetic response to each drug in a synergistic pair is enriched for overlapping genes (Jansen et al., 2009).

This overlap in responsive gene sets led us to consider the possibility that overlapping responsive genes from known synergistic compound pairs could be used as biomarkers to predict new synergistic combinations. Our method involves first identifying the overlaps in responsive gene sets for all compounds that had been reported in the literature to synergize with a small molecule of interest ("compound X"), selecting those genes common to all of those sets (Figure 6A, middle, the overlaps of overlaps). We refer to these genes as "synergy biomarker genes." Critically, we next hypothesized that any compound that contains one or more of these synergy biomarker genes in its responsive gene set would be synergistic with compound X. Because our method used the overlaps of response gene overlaps between compounds known to be synergistic, we refer to it as the "overlap-squared method" or "O2M."

We then tested O2M using two drugs for which substantial literature synergy information was available: FLC and geldanamycin (GdA). FLC is an approved antifungal drug. GdA is an inhibitor of Hsp90, a chaperone protein with many physical and genetic interactions (Taipale et al., 2010). We performed our analysis on fenpropimorph and sertraline, which are known to

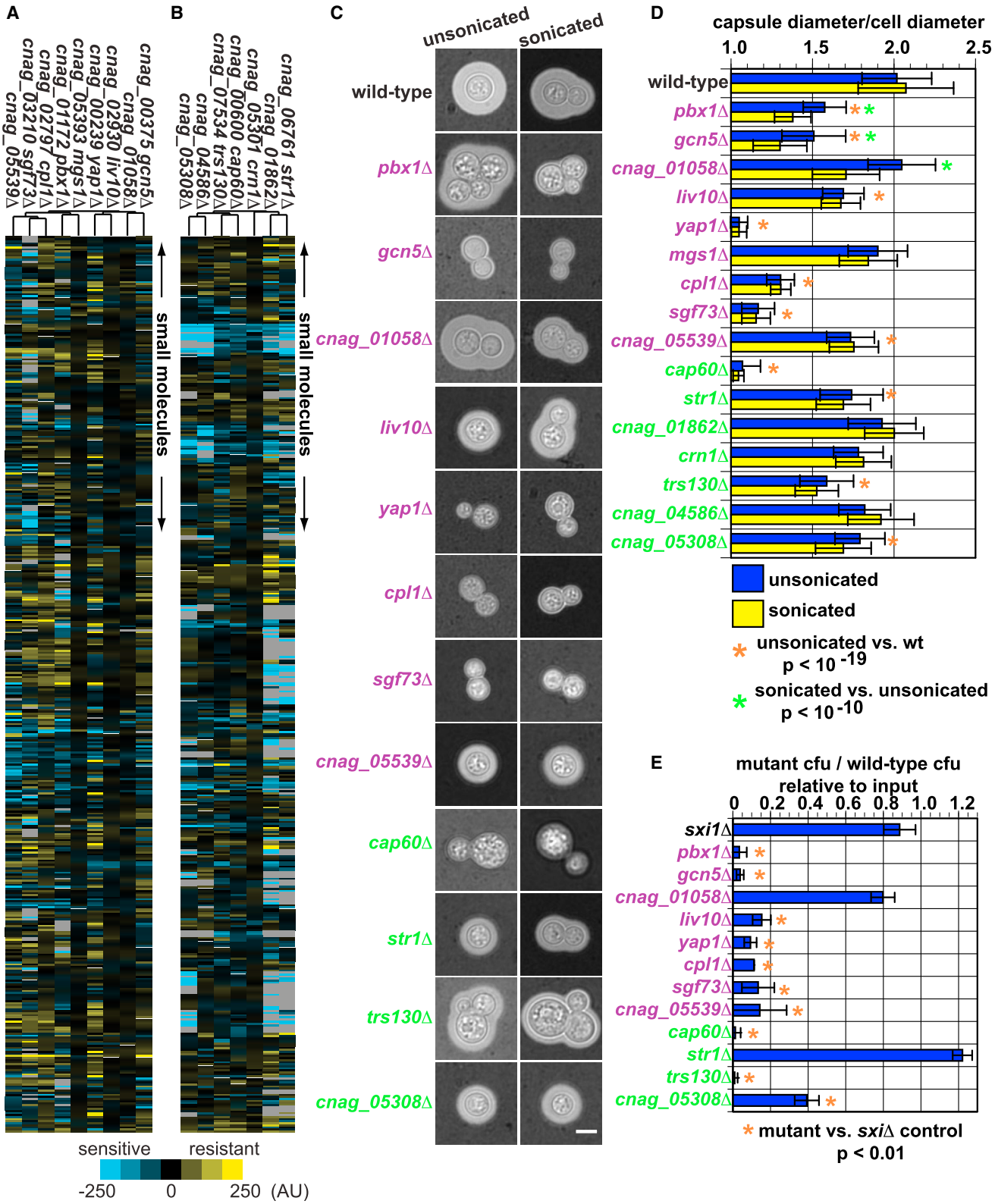

Figure 4. Chemical-Genetic Profiling Identifies Genes Involved in Capsule Biosynthesis

(A) Cluster containing the chemical signatures of the *pbx1*Δ and *cpl1*Δ mutants.

(B) Cluster containing the chemical signatures of the *cap60*Δ mutants.

(legend continued on next page)

act synergistically with FLC (Jansen et al., 2009; Zhai et al., 2012), and cyclosporine and rapamycin, which are known to act synergistically with GdA (Francis et al., 2006; Kumar et al., 2005). Using this prior knowledge and our data, we identified synergy biomarker genes for FLC (*CNAG_00573*, *CNAG_03664*, and *CNAG_03917*) and GdA (*CNAG_01172*, *CNAG_03829*, and *CNAG_01862*). We generated a list of compounds from our chemical-genetics data set that contain one or more of these genes in their responsive genes set.

We then used a standard ''checkerboard'' assay to experimentally determine fractional inhibitory concentration index (FICI), and we adopted the standard that an FICI value below 0.5 is synergistic (Meletiadis et al., 2010). We determined FICIs for FLC and GdA with three sets of compounds: (1) the compounds predicted from synergy biomarker genes, (2) the predicted synergistic compounds for the other drug (e.g., we tested compounds predicted to be synergistic with GdA for synergy with FLC), and (3) a randomly generated subset of the compounds not predicted to act synergistically with either FLC or GdA. The second and third groups are as controls for compounds that are generally synergistic and to determine the background frequency of synergistic interactions within a set of compounds.

Respective experimental FICI values for FLC and GdA are shown in Figures 6B and 6C (yellow bars: synergy; blue bars additive or worse interactions). The labels for compounds we predicted to be synergistic are colored purple, positive controls (published synergistic compound pairs) are colored green, and predicted negative control compounds are colored blue (Figure 6). We observed that only ~10% of the negative control compounds act synergistically with either FLC or GdA. In striking contrast, we found ~80% and ~60% of the compounds selected by O2M are synergistic with FLC and GdA, respectively. Thus, for two unrelated compounds, O2M is highly successful at predicting synergistic interactions and performs vastly better than the brute force trial-and-error approach (Figures 6D and 6E) ($p < 0.0008$, Fisher's exact test).

DISCUSSION

We applied chemogenomic profiling to the major fungal driver of AIDS-related death, the encapsulated yeast *C. neoformans,* to produce a chemical-genetic atlas of this important pathogen. Beyond identifying new virulence factors and compound mode of action, we describe a conceptually general approach to identifying drug synergies that combines prior knowledge and chemogenomic profiles.

A Chemical-Genetic Atlas for *C. neoformans*

We maximized the quality of the atlas in several ways. To capture concentration-dependent impacts of compounds, we obtained the MIC for each compound and examined the genetic responses at multiple concentrations below MIC. In addition, we performed a large number of control screens and incorporated batch information for systematic correction. Overall benchmarks of data quality (Figure 1) together with nearest neighbor and Gene Ontology analysis (Figure 2) support the existence of substantial chemical-genetic signal in the data. Even genes with orthologs in both *S. cerevisiae* and *C. neoformans* show considerable differences in responses (Figure 3). While this may not be surprising given the large phylogenetic distance between these fungi, it shows that understanding the chemical responses of pathogens requires pathogen-focused studies, even when considering conserved genes and processes. For example, we observed differences in the responses to azole drugs between *S. cerevisiae* and *C. neoformans* (Figure 3). Since azoles are heavily used clinically, differences in responses between species are of significant interest.

Insights Gained from Initial Use of the *C. neoformans* Chemical-Genetic Atlas

Identification of Mutants that Impact Capsule Formation and Mammalian Infection

Our studies on capsule biosynthesis genes focused two different clusters that contained genes that we and others have shown to be required for capsule formation, the *pbx1/cpl1Δ* cluster and the *cap60Δ* cluster. As anticipated from model organism studies (Collins et al., 2007; Costanzo et al., 2010; Nichols et al., 2011; Parsons et al., 2004; Parsons et al., 2006), these clusters were indeed enriched for genes whose mutants are defective in capsule biosynthesis and mammalian pathogenesis. The genes represented by the two clusters differed functionally in that genes in the *pbx1/cpl1Δ* cluster but not the *cap60Δ* cluster are required for association of capsule polysaccharide with the cell surface (Figures 4 and S2). A recent study on Pbx1 and its ortholog, Pbx2, proposes that the two proteins act redundantly in capsule assembly (Kumar et al., 2014). *pbx1*Δ and *pbx2*Δ cells shed lower amounts of GXM into the culture medium but that the GXM functions in a capsule transfer assay. Electron microscopy studies indicate that these mutants exhibit defects in the cell wall. Our data are fully consistent with these data. Other genes from the *pbx1Δ/cpl1Δ* cluster likely play a role in these processes. Some, like *GCN5* and *SGF73*, which encode orthologs of the yeast SAGA histone acetylase/deubiquitylase complex, are clearly regulatory, while others could act more directly. While detailed validation and investigation of these many candidates (including gene deletion reconstruction studies) will be required to obtain mechanistic insight into capsule biology, their enrichment suggests value of this Cryptococcal chemogenomic resource in identifying mutants defective in virulence.

Compound Target Identification

Chemogenomic profiling has proven useful in identifying targets of uncharacterized compounds (Parsons et al., 2006), including

(C) Images of individual cells grown in 10% Sabouraud's broth to induce capsule. Representative cells are shown for mutants that exhibit a statistically significant phenotype. Scale bar, 5 μm.

(D) Quantification of capsule sizes from all mutants in *pbx1*Δ/*cpl1*Δ (purple labels) cluster or *cap60*Δ (green labels) cluster. 100 cells were measured for each strain, the error bars represents the standard deviation, and p values were calculated using Student's t test.

(E) Colony counts from colony forming units (cfu) extracted from mouse lungs following an inhalation infection. Three mice are shown for each datapoint; the error bars represent the standard deviation and p values were calculated using Student's t test.

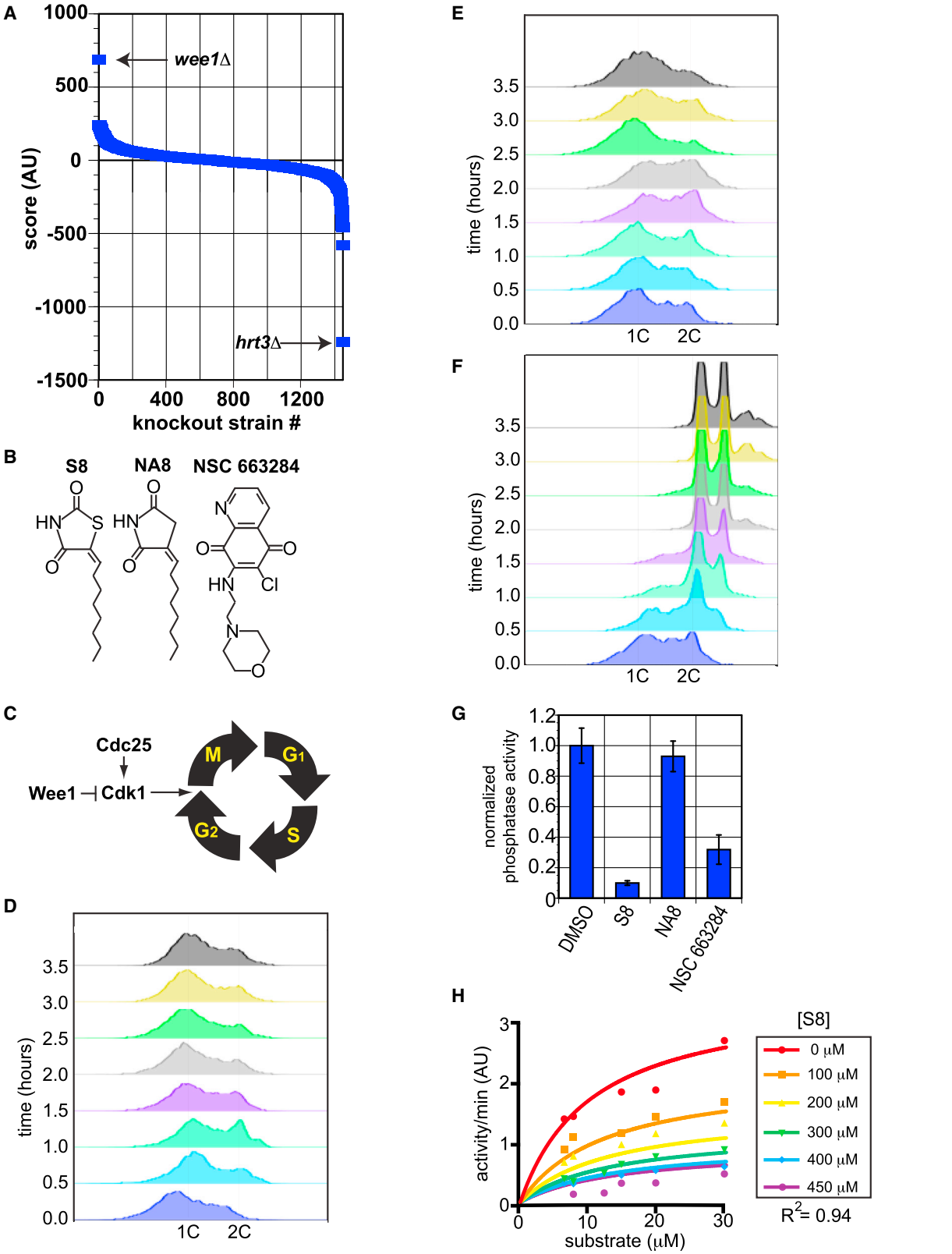

(legend on next page)

in the pathogenic fungus *C. albicans* (Jiang et al., 2008; Xu et al., 2007; Xu et al., 2009). Chemical-genetic data can be used to determine the target of compounds within complex mixtures (Jiang et al., 2008; Xu et al., 2009). Our goal differed: we sought to identify targets of repurposed compounds, as described elsewhere (Butts et al., 2013), or, in the case of S8, a compound identified as an inhibitor of *Candida* biofilms (Kagan et al., 2014). The identification of the Wee1 kinase as a sensitivity determinant for S8, the cell-cycle arrest produced by S8, and the ability of the compound to inhibit *Cn*Cdc25 in vitro together support the model that S8 inhibits growth through via the cell cycle at least in part via inhibition of Cdc25. Whether this explains its impact on biofilms requires further investigation. As with any compound target, ultimate proof that Cdc25 is the target of S8 will require the isolation of resistance alleles of *CDC25*.

Given the simplicity of the pharmacophore and its K_i for *Cn*Cdc25, it would not be surprising if S8 had additional cellular targets, as recently described (Feldman et al., 2014). Cdc25 is a conserved cell-cycle phosphatase and therefore might be considered a poor drug target a priori but cyclin-dependent kinases are a focus of recent antiparasite therapeutics (Geyer et al., 2005). It is also notable that the target of azole antifungals, lanosterol 14-demethylase (Ghannoum and Rice, 1999) is conserved from yeast to human.

O2M: Predicting Compound Synergies Using Prior Knowledge and Chemical Profiles

Identifying synergistic drug interactions is of considerable clinical interest, but efficient methods for their identification are elusive. Systematic examination of combinations of a small set of compounds using *S. cerevisiae* suggests that synergies are relatively rare and often involve so-called "promiscuous" synergizers, compounds that are synergistic with multiple partners (Cokol et al., 2011). Chemogenomic studies have shown that drugs known to be synergistic tend to have overlapping "responding" gene sets (Jansen et al., 2009). We expanded on this concept to develop a highly parallel method, O2M, for efficiently predicting synergistic drug interactions. Our work utilizes prior knowledge of drug synergies to identify a discrete set of predictive biomarker genes for a given compound. We experimentally demonstrated the utility of O2M for two compounds, FLC and geldanamycin. Our method identified dozens of synergistic interactions and discovered a small number of biomarkers that could serve as readouts for further screens for synergistic drugs. The method appears to not simply select promiscuous synergiziers: five of six drugs previously classified as promiscuous synergizers (Cokol et al., 2011) were tested in our studies but most were not predicted to be synergistic by O2M. One of the promiscuous compounds was a positive control (fenpropimorph with FLC) and another (dyclonine) was predicted synergistic with FLC but was not and was predicted not synergistic with GdA but was. We anticipate that O2M could be used to identify synergistic compound interactions in published *E. coli* and *C. albicans* chemical-genetics data sets (Jiang et al., 2008; Nichols et al., 2011; Xu et al., 2007; Xu et al., 2009).

EXPERIMENTAL PROCEDURES

Determination of MICs

We determined MIC on solid growth medium for each compound used in screening (Table 1).

Colony Array-Based Chemogenomic Profiling

C. neoformans knockouts were inoculated from frozen 384-well plates to YNB + 2% glucose. Plates were grown 24 hr at 30°C, then used to inoculate screening plates containing compounds of interest.

Data Analysis

Data were analyzed as previously described (Baryshnikova et al., 2010) with the a few exceptions.

C. neoformans Ortholog Identification and GO Term Mapping

Mapping from *S. cerevisiae* Uniprot Proteins to *C. neoformans* Uniprot Proteins was done using One-to-one mappings in MetaPhOrs (http://metaphors.phylomedb.org/). *C. neoformans* ORFs were compared to a database of *S. cerevisiae* Uniprot Proteins using blastp (Altschul et al., 1997) with a E-score cutoff of 10^{-30}. Corresponding yeast GO annotations were mapped onto the *C. neoformans* ORFs.

Comparison of Transcriptional Response to FLC

Compared transcriptional responses between *S. cerevisiae* (Kuo et al., 2010) and *C. neoformans* (Florio et al., 2011).

Capsule Induction Assay

Samples were grown overnight at 30°C in 100% Sabouraud's broth, then diluted 1:100 into 10% Sabouraud's broth buffered with 50 mM HEPES pH 7.3 and grown for 3 days at 37°C. India ink was added at 3:1 ratio and samples imaged on a Zeiss Axiovert microscope.

Capsule Transfer Assay

Performed as in (Reese and Doering, 2003), with minor modifications.

GXM Immunoblot Assay

Conditioned medium was made from donor GXM donor strains as described above.

Figure 5. *C. neoformans* Cdc25 Is a Target of S8 In Vivo and In Vitro

(A) Chemical-genetic data of the growth scores of each knockout mutant grown on S8 (y axis). The mutant that exhibited the greatest resistance is *wee1*Δ. The mutant strain that showed the greatest sensitivity to S8 is *cnag_04462*Δ.

(B) Structures of S8, NA8, and NSC 663284. The structure of S10 is shown in Figure S3C.

(C) G2/M regulation (Morgan, 2007).

(D) DNA content of asynchronous *C. neoformans* culture split into aliquots for treatment with compounds of interest, with samples harvested at appropriate times. Data for DMSO-treated culture is shown.

(E) DNA content from NA8-treated culture from same starting culture as Figure 5F.

(F) DNA content from S8-treated culture from same starting culture as Figure 5F.

(G) Phosphatase activity of purified C. neoformans Cdc25 catalytic domain (CNAG_01572, aa442-662). Average of three independent replicates are shown and the error bars represent the standard deviation.

(H) Michaelis-Menten kinetics of S8 inhibition of *Cn*Cdc25 from in vitro phosphatase activity. A noncompetitive model of enzyme inhibition produced the best R^2 value (0.94).

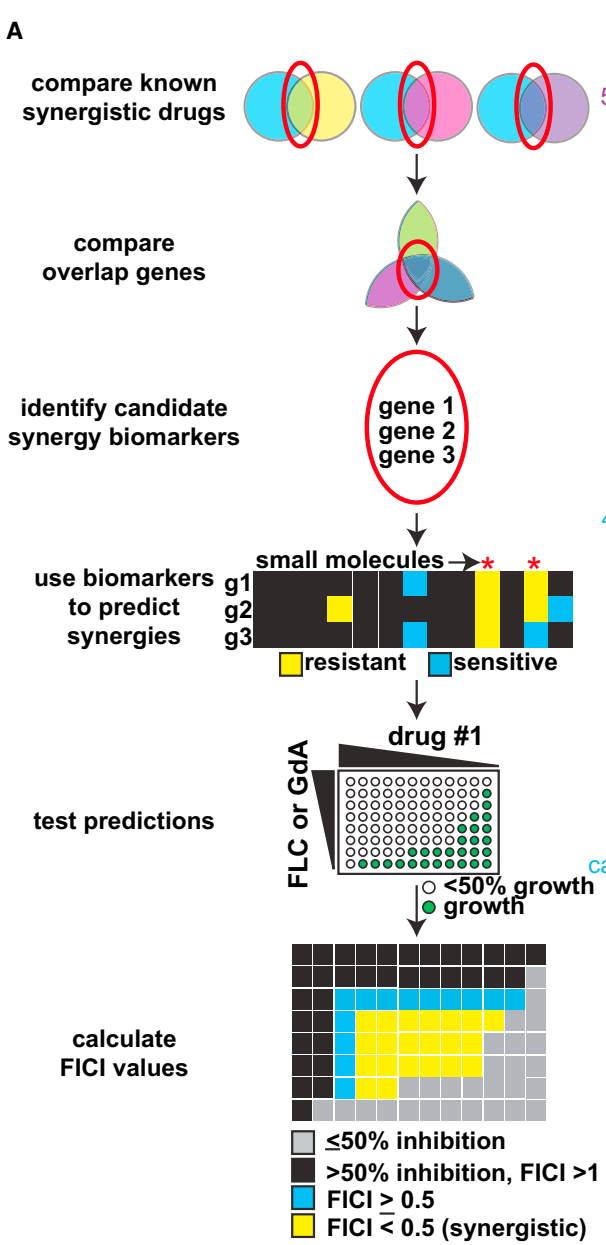

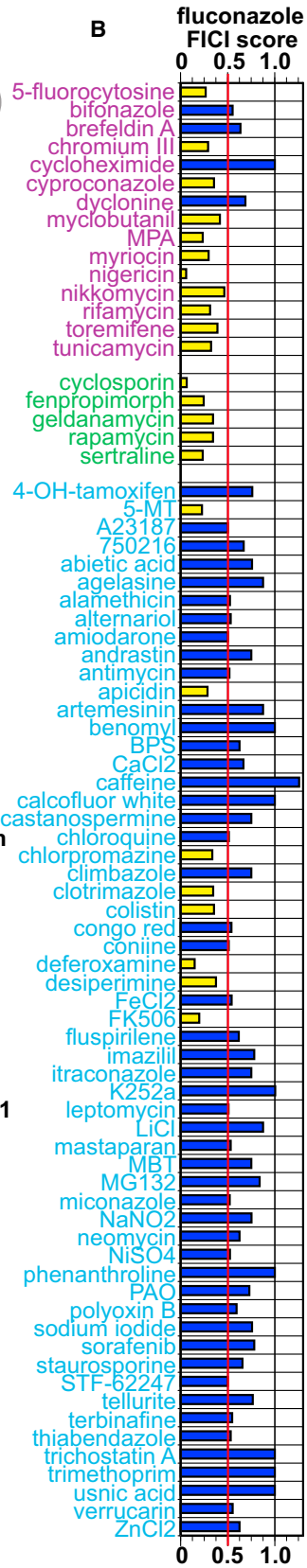

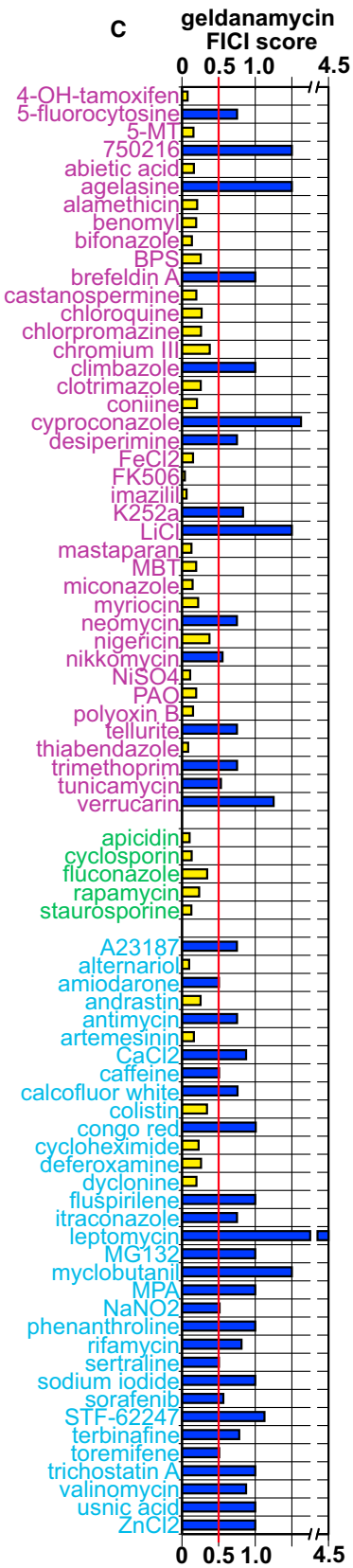

D

fluconazole	predicted synergistic	negative controls
synergistic	11	8
not synergistic	4	50

E

geldanamycin	predicted synergistic	negative controls
synergistic	25	6
not synergistic	15	26

(legend on next page)

Mouse Infection Assay

Mouse lung infections were performed as previously described (Chun et al., 2011).

Cdc25 Protein Purification

We identified the *C.* neoformans ortholog of Cdc25, *CNAG_01572*, by best reciprocal BLAST (Altschul et al., 1997) hit with the human Cdc25A, Cdc25B, and Cdc25C protein isoforms. We then inserted the exonic sequence of the catalytic domain into a 6×-His tag expression vector for purification.

Cdc25 Phosphatase Assay

Cdc25 phosphatase activity was analyzed in activity buffer (50 mM Tris pH 8.3, 5% glycerol, 0.8 mM dithiolthreitol, and 1% PVA).

Cdc25 Inhibitor Treatment and FACS Analysis

Wild-type *C. neoformans* was grown overnight in 1× YNB at 30°C with rotation. Cultures were diluted to OD_{600} ~0.2 into 150 ml 1× YNB, then incubated 3 hr at 30°C. Samples were then split and NA8, S8, and S10 added to 60 μM. Equivalent volume of DMSO was added to the control culture.

Fractional Inhibitory Concentration Index Assay for Synergy

We determined FICI using a standard checkerboard assay (Hsieh et al., 1993), calculating FICI as described using a 50% growth inhibition cutoff for MICs for individual compounds (Hsieh et al., 1993; Meletiadis et al., 2010), then using a standard cutoff of FICI < 0.5 to define synergy.

See Extended Experimental Procedures for additional details.

SUPPLEMENTAL INFORMATION

Supplemental Information includes Extended Experimental Procedures, three figures, and seven tables and can be found with this article online at http://dx.doi.org/10.1016/j.cell.2014.10.044.

AUTHOR CONTRIBUTIONS

J.C.S.B. and H.D.M. designed the study. J.C.S.B. carried out all of experiments described in the paper. J.N. and C.L.M. performed data analysis shown in Figures 1B–1D, Figure 2 and Figure 3. B.V., R.D., and C.L.M. filtered, denoised and scored the primary colony array data. A.B., S.K., I.P., and D.J.K. provided compounds and guidance. J.C.S.B. and H.D.M. wrote the manuscript with input from all coauthors.

ACKNOWLEDGMENTS

This work was supported by NIH grants 5R01AI099206 to H.D.M., 1R01AI091422 to D.J.K., 1R01HG005084 and 1R01GM04975 to C.L.M, and a grant from the CIFAR Genetic Networks Program to C.L.M.

Received: July 3, 2014
Revised: August 28, 2014
Accepted: October 22, 2014
Published: November 20, 2014

REFERENCES

Altschul, S.F., Madden, T.L., Schäffer, A.A., Zhang, J., Zhang, Z., Miller, W., and Lipman, D.J. (1997). Gapped BLAST and PSI-BLAST: a new generation of protein database search programs. Nucleic Acids Res. *25*, 3389–3402.

Anderson, J.B. (2005). Evolution of antifungal-drug resistance: mechanisms and pathogen fitness. Nat. Rev. Microbiol. *3*, 547–556.

Armstrong-James, D., Meintjes, G., and Brown, G.D. (2014). A neglected epidemic: fungal infections in HIV/AIDS. Trends Microbiol. *22*, 120–127.

Baryshnikova, A., Costanzo, M., Kim, Y., Ding, H., Koh, J., Toufighi, K., Youn, J.-Y., Ou, J., San Luis, B.-J., Bandyopadhyay, S., et al. (2010). Quantitative analysis of fitness and genetic interactions in yeast on a genome scale. Nat. Methods *7*, 1017–1024.

Broek, D., Bartlett, R., Crawford, K., and Nurse, P. (1991). Involvement of p34cdc2 in establishing the dependency of S phase on mitosis. Nature *349*, 388–393.

Butts, A., and Krysan, D.J. (2012). Antifungal drug discovery: something old and something new. PLoS Pathog. *8*, e1002870.

Butts, A., DiDone, L., Koselny, K., Baxter, B.K., Chabrier-Rosello, Y., Wellington, M., and Krysan, D.J. (2013). A repurposing approach identifies off-patent drugs with fungicidal cryptococcal activity, a common structural chemotype, and pharmacological properties relevant to the treatment of cryptococcosis. Eukaryot. Cell *12*, 278–287.

Butts, A., Koselny, K., Chabrier-Roselló, Y., Semighini, C.P., Brown, J.C.S., Wang, X., Annadurai, S., DiDone, L., Tabroff, J., Childers, W.E., Jr., et al. (2014). Estrogen receptor antagonists are anti-cryptococcal agents that directly bind EF hand proteins and synergize with fluconazole in vivo. MBio *5*, e00765–e13.

Cantas, L., Shah, S.Q.A., Cavaco, L.M., Manaia, C.M., Walsh, F., Popowska, M., Garelick, H., Bürgmann, H., and Sørum, H. (2013). A brief multi-disciplinary review on antimicrobial resistance in medicine and its linkage to the global environmental microbiota. Front Microbiol *4*, 96.

Chang, Y.C., and Kwon-Chung, K.J. (1998). Isolation of the third capsule-associated gene, CAP60, required for virulence in Cryptococcus neoformans. Infect. Immun. *66*, 2230–2236.

Chun, C.D., Brown, J.C.S., and Madhani, H.D. (2011). A major role for capsule-independent phagocytosis-inhibitory mechanisms in mammalian infection by Cryptococcus neoformans. Cell Host Microbe *9*, 243–251.

Cokol, M., Chua, H.N., Tasan, M., Mutlu, B., Weinstein, Z.B., Suzuki, Y., Nergiz, M.E., Costanzo, M., Baryshnikova, A., Giaever, G., et al. (2011). Systematic exploration of synergistic drug pairs. Mol. Syst. Biol. *7*, 544.

Collins, S.R., Miller, K.M., Maas, N.L., Roguev, A., Fillingham, J., Chu, C.S., Schuldiner, M., Gebbia, M., Recht, J., Shales, M., et al. (2007). Functional dissection of protein complexes involved in yeast chromosome biology using a genetic interaction map. Nature *446*, 806–810.

Costanzo, M., Baryshnikova, A., Bellay, J., Kim, Y., Spear, E.D., Sevier, C.S., Ding, H., Koh, J.L.Y., Toufighi, K., Mostafavi, S., et al. (2010). The genetic landscape of a cell. Science *327*, 425–431.

Del Poeta, M. (2004). Role of phagocytosis in the virulence of Cryptococcus neoformans. Eukaryot. Cell *3*, 1067–1075.

Figure 6. O2M Approach for Predicting Compound Synergy

(A) Approach for predicting compound synergistic interaction.

(B) FICI values for fluconazole (FLC). Predicted synergistic compounds are labeled in purple and known synergistic compounds in green. Bars represent the average of two assays but both had to be FICI < 0.5 to be considered synergistic. Compounds labeled in blue are negative controls from one of two categories: 1) predicted to synergize with geldanamycin (GdA) but not FLC or 2) randomly generated list of compounds not predicted to be synergistic with either FLC or GdA. Yellow bars represent an FICI < 0.5 (synergistic) and blue bars and FICI ≥ 0.5 (not synergistic).

(C) FICI values for GdA. Labels and colors are analogous to those in part B.

(D) Contingency table of synergistic versus nonsynergistic interactions with FLC. $p < 0.0008$ (Fisher's exact test).

(E) Contingency table of synergistic versus nonsynergistic interactions with GdA. $p < 0.0008$ (Fisher's exact test).

Dittmar, J.C., Reid, R.J., and Rothstein, R. (2010). ScreenMill: a freely available software suite for growth measurement, analysis and visualization of high-throughput screen data. BMC Bioinformatics *11*, 353–363.

Doering, T.L. (2009). How sweet it is! Cell wall biogenesis and polysaccharide capsule formation in Cryptococcus neoformans. Annu. Rev. Microbiol. *63*, 223–247.

Feldman, M., Al-Quntar, A., Polacheck, I., Friedman, M., and Steinberg, D. (2014). Therapeutic potential of thiazolidinedione-8 as an antibiofilm agent against *Candida albicans*. PLoS ONE *9*, e93225.

Fernández, L., and Hancock, R.E.W. (2012). Adaptive and mutational resistance: role of porins and efflux pumps in drug resistance. Clin. Microbiol. Rev. *25*, 661–681.

Florio, A.R., Ferrari, S., De Carolis, E., Torelli, R., Fadda, G., Sanguinetti, M., Sanglard, D., and Posteraro, B. (2011). Genome-wide expression profiling of the response to short-term exposure to fluconazole in Cryptococcus neoformans serotype A. BMC Microbiol. *11*, 97.

Francis, L.K., Alsayed, Y., Leleu, X., Jia, X., Singha, U.K., Anderson, J., Timm, M., Ngo, H., Lu, G., Huston, A., et al. (2006). Combination mammalian target of rapamycin inhibitor rapamycin and HSP90 inhibitor 17-allylamino-17-demethoxygeldanamycin has synergistic activity in multiple myeloma. Clin. Cancer Res. *12*, 6826–6835.

Geyer, J.A., Prigge, S.T., and Waters, N.C. (2005). Targeting malaria with specific CDK inhibitors. Biochim. Biophys. Acta *1754*, 160–170.

Ghannoum, M.A., and Rice, L.B. (1999). Antifungal agents: mode of action, mechanisms of resistance, and correlation of these mechanisms with bacterial resistance. Clin. Microbiol. Rev. *12*, 501–517.

Haynes, B.C., Skowyra, M.L., Spencer, S.J., Gish, S.R., Williams, M., Held, E.P., Brent, M.R., and Doering, T.L. (2011). Toward an integrated model of capsule regulation in *Cryptococcus neoformans*. PLoS Pathog. *7*, e1002411.

Heitman J., Kozel T.R., Kwon-Chung K.J., Perfect J.R., and Casadevall A., eds. (2011). Cryptococcus: from human pathogen to model yeast (Washington, D.C.: ASM Press).

Hill, H.D., Summer, G.K., and Waters, M.D. (1968). An automated fluorometric assay for alkaline phosphatase using 3-O-methylfluorescein phosphate. Anal. Biochem. *24*, 9–17.

Hillenmeyer, M.E., Fung, E., Wildenhain, J., Pierce, S.E., Hoon, S., Lee, W., Proctor, M., St Onge, R.P., Tyers, M., Koller, D., et al. (2008). The chemical genomic portrait of yeast: uncovering a phenotype for all genes. Science *320*, 362–365.

Hsieh, M.H., Yu, C.M., Yu, V.L., and Chow, J.W. (1993). Synergy assessed by checkerboard. A critical analysis. Diagn. Microbiol. Infect. Dis. *16*, 343–349.

Janbon, G., Ormerod, K.L., Paulet, D., Byrnes, E.J., 3rd, Yadav, V., Chatterjee, G., Mullapudi, N., Hon, C.-C., Billmyre, R.B., Brunel, F., et al. (2014). Analysis of the genome and transcriptome of *Cryptococcus neoformans* var. *grubii* reveals complex RNA expression and microevolution leading to virulence attenuation. PLoS Genet. *10*, e1004261.

Jansen, G., Lee, A.Y., Epp, E., Fredette, A., Surprenant, J., Harcus, D., Scott, M., Tan, E., Nishimura, T., Whiteway, M., et al. (2009). Chemogenomic profiling predicts antifungal synergies. Mol. Syst. Biol. *5*, 338.

Jiang, B., Xu, D., Allocco, J., Parish, C., Davison, J., Veillette, K., Sillaots, S., Hu, W., Rodriguez-Suarez, R., Trosok, S., et al. (2008). PAP inhibitor with in vivo efficacy identified by Candida albicans genetic profiling of natural products. Chem. Biol. *15*, 363–374.

Kagan, S., Jabbour, A., Sionov, E., Alquntar, A.A., Steinberg, D., Srebnik, M., Nir-Paz, R., Weiss, A., and Polacheck, I. (2014). Anti-Candida albicans biofilm effect of novel heterocyclic compounds. J. Antimicrob. Chemother. *69*, 416–427.

Kalan, L., and Wright, G.D. (2011). Antibiotic adjuvants: multicomponent anti-infective strategies. Expert Rev. Mol. Med. *13*, e5.

Kathiravan, M.K., Salake, A.B., Chothe, A.S., Dudhe, P.B., Watode, R.P., Mukta, M.S., and Gadhwe, S. (2012). The biology and chemistry of antifungal agents: a review. Bioorg. Med. Chem. *20*, 5678–5698.

Kozel, T.R., and Hermerath, C.A. (1984). Binding of cryptococcal polysaccharide to Cryptococcus neoformans. Infect. Immun. *43*, 879–886.

Kozel, T.R., Levitz, S.M., Dromer, F., Gates, M.A., Thorkildson, P., and Janbon, G. (2003). Antigenic and biological characteristics of mutant strains of Cryptococcus neoformans lacking capsular O acetylation or xylosyl side chains. Infect. Immun. *71*, 2868–2875.

Kumar, R., Musiyenko, A., and Barik, S. (2005). Plasmodium falciparum calcineurin and its association with heat shock protein 90: mechanisms for the antimalarial activity of cyclosporin A and synergism with geldanamycin. Mol. Biochem. Parasitol. *141*, 29–37.

Kumar, P., Yang, M., Haynes, B.C., Skowyra, M.L., and Doering, T.L. (2011). Emerging themes in cryptococcal capsule synthesis. Curr. Opin. Struct. Biol. *21*, 597–602.

Kumar, P., Heiss, C., Santiago-Tirado, F.H., Black, I., Azadi, P., and Doering, T.L. (2014). Pbx proteins in Cryptococcus neoformans cell wall remodeling and capsule assembly. Eukaryot. Cell *13*, 560–571.

Kuo, D., Tan, K., Zinman, G., Ravasi, T., Bar-Joseph, Z., and Ideker, T. (2010). Evolutionary divergence in the fungal response to fluconazole revealed by soft clustering. Genome Biol. *11*, R77.

Lehár, J., Krueger, A.S., Avery, W., Heilbut, A.M., Johansen, L.M., Price, E.R., Rickles, R.J., Short, G.F., 3rd, Staunton, J.E., Jin, X., et al. (2009). Synergistic drug combinations tend to improve therapeutically relevant selectivity. Nat. Biotechnol. *27*, 659–666.

Liu, C., Apodaca, J., Davis, L.E., and Rao, H. (2007a). Proteasome inhibition in wild-type yeast *Saccharomyces cerevisiae* cells. Biotechniques *42*, 158–162, 160, 162.

Liu, O.W., Kelly, M.J.S., Chow, E.D., and Madhani, H.D. (2007b). Parallel β-helix proteins required for accurate capsule polysaccharide synthesis and virulence in the yeast Cryptococcus neoformans. Eukaryot. Cell *6*, 630–640.

Liu, O.W., Chun, C.D., Chow, E.D., Chen, C., Madhani, H.D., and Noble, S.M. (2008). Systematic genetic analysis of virulence in the human fungal pathogen *Cryptococcus neoformans*. Cell *135*, 174–188.

Loyse, A., Bicanic, T., and Jarvis, J.N. (2013). Combination antifungal therapy for cryptococcal meningitis. N. Engl. J. Med. *368*, 2522–2523.

Lozano, R., Naghavi, M., Foreman, K., Lim, S., Shibuya, K., Aboyans, V., Abraham, J., Adair, T., Aggarwal, R., Ahn, S.Y., et al. (2012). Global and regional mortality from 235 causes of death for 20 age groups in 1990 and 2010: a systematic analysis for the Global Burden of Disease Study 2010. Lancet *380*, 2095–2128.

Mandell, G.L., Bennett, J.E., and Dolin, R. (2010). Mandell, Douglas, and Bennett's Principles and Practice of Infectious Diseases, 7th edn (Philadelphia: Churchill Livingstone Elsevier).

Meletiadis, J., Pournaras, S., Roilides, E., and Walsh, T.J. (2010). Defining fractional inhibitory concentration index cutoffs for additive interactions based on self-drug additive combinations, Monte Carlo simulation analysis, and in vitro-in vivo correlation data for antifungal drug combinations against Aspergillus fumigatus. Antimicrob. Agents Chemother. *54*, 602–609.

Morgan, D.O. (2007). The Cell Cycle: Principles of Control (London, UK: New Science Press).

Nichols, R.J., Sen, S., Choo, Y.J., Beltrao, P., Zietek, M., Chaba, R., Lee, S., Kazmierczak, K.M., Lee, K.J., Wong, A., et al. (2011). Phenotypic landscape of a bacterial cell. Cell *144*, 143–156.

O'Meara, T.R., and Alspaugh, J.A. (2012). The Cryptococcus neoformans capsule: a sword and a shield. Clin. Microbiol. Rev. *25*, 387–408.

O'Meara, T.R., Norton, D., Price, M.S., Hay, C., Clements, M.F., Nichols, C.B., and Alspaugh, J.A. (2010). Interaction of Cryptococcus neoformans Rim101 and protein kinase A regulates capsule. PLoS Pathog. *6*, e1000776.

Park, B.J., Wannemuehler, K.A., Marston, B.J., Govender, N., Pappas, P.G., and Chiller, T.M. (2009). Estimation of the current global burden of cryptococcal meningitis among persons living with HIV/AIDS. AIDS *23*, 525–530.

Parsons, A.B., Brost, R.L., Ding, H., Li, Z., Zhang, C., Sheikh, B., Brown, G.W., Kane, P.M., Hughes, T.R., and Boone, C. (2004). Integration of chemical-genetic and genetic interaction data links bioactive compounds to cellular target pathways. Nat. Biotechnol. *22*, 62–69.

Parsons, A.B., Lopez, A., Givoni, I.E., Williams, D.E., Gray, C.A., Porter, J., Chua, G., Sopko, R., Brost, R.L., Ho, C.-H., et al. (2006). Exploring the mode-of-action of bioactive compounds by chemical-genetic profiling in yeast. Cell *126*, 611–625.

Pu, L., Amoscato, A.A., Bier, M.E., and Lazo, J.S. (2002). Dual G1 and G2 phase inhibition by a novel, selective Cdc25 inhibitor 6-chloro-7-[corrected](2-morpholin-4-ylethylamino)-quinoline-5,8-dione. J. Biol. Chem. *277*, 46877–46885.

Reese, A.J., and Doering, T.L. (2003). Cell wall α-1,3-glucan is required to anchor the Cryptococcus neoformans capsule. Mol. Microbiol. *50*, 1401–1409.

Roemer, T., Xu, D., Singh, S.B., Parish, C.A., Harris, G., Wang, H., Davies, J.E., and Bills, G.F. (2011). Confronting the challenges of natural product-based antifungal discovery. Chem. Biol. *18*, 148–164.

Taipale, M., Jarosz, D.F., and Lindquist, S. (2010). HSP90 at the hub of protein homeostasis: emerging mechanistic insights. Nat. Rev. Mol. Cell Biol. *11*, 515–528.

Vecchiarelli, A., Pericolini, E., Gabrielli, E., Kenno, S., Perito, S., Cenci, E., and Monari, C. (2013). Elucidating the immunological function of the Cryptococcus neoformans capsule. Future Microbiol. *8*, 1107–1116.

Whelan, W.L., and Kwon-Chung, K.J. (1986). Genetic complementation in Cryptococcus neoformans. J. Bacteriol. *166*, 924–929.

WHO (2011). Rapid Advice: diagnosis, prevention and management of cryptococcal disease in HIV-infected adults, adolescents, and children, W.H.O. Library, ed. (Geneva, Switzerland: WHO Press).

Xu, D., Jiang, B., Ketela, T., Lemieux, S., Veillette, K., Martel, N., Davison, J., Sillaots, S., Trosok, S., Bachewich, C., et al. (2007). Genome-wide fitness test and mechanism-of-action studies of inhibitory compounds in Candida albicans. PLoS Pathog. *3*, e92.

Xu, D., Sillaots, S., Davison, J., Hu, W., Jiang, B., Kauffman, S., Martel, N., Ocampo, P., Oh, C., Trosok, S., et al. (2009). Chemical genetic profiling and characterization of small-molecule compounds that affect the biosynthesis of unsaturated fatty acids in Candida albicans. J. Biol. Chem. *284*, 19754–19764.

Zhai, B., Wu, C., Wang, L., Sachs, M.S., and Lin, X. (2012). The antidepressant sertraline provides a promising therapeutic option for neurotropic cryptococcal infections. Antimicrob. Agents Chemother. *56*, 3758–3766.

EXTENDED EXPERIMENTAL PROCEDURES

Minimal Inhibitory Concentration Determination

We determined the MIC on solid growth medium for each small molecule used in screening. Small-molecule solutions were serially diluted two-fold in yeast nitrogen base (YNB) with 2% glucose and 2% agar, inoculated with wild-type *C. neoformans*, then grown 24 hr at 30°C. The MIC is the lowest concentration of small molecule that completely inhibits growth. Screens were performed at 50%, 25%, and 12.5% the MIC.

Chemogenomic Profiling

The *C. neoformans* knockout collection was inoculated from frozen 384-well plates to YNB + 2% glucose. Plates were grown 24 hr at 30°C, then used to inoculate screening plates containing small molecules of interest. Up to six screening plates were inoculated from a single YNB source plate. Source plates were grown 24 hr between inoculations, used a maximum of three times, and passaged no more than twice. Plates were pinned in duplicate from two different 384-colony source plates to 1,536-colony testing plates containing 1× YNB + 2% glucose + 2% agar + small molecule, grown 24 hr at 30°C, then scanned on a flatbed scanner with autofocus. Colony size data were extracted using ScreenMill (Dittmar et al., 2010).

Data Analysis

Plate data were visually examined and entire plates or plate regions were removed if they were determined to have problems (e.g., spatial effects) too severe for automatic correction. Data were analyzed as previously described (Baryshnikova et al., 2010) with the a few exceptions. First, because each 1,536-well plate was pinned from interleaved 384-well sources, an additional round of spatial correction and plate normalization was applied to each of these components individually before initial plate-wide normalization and spatial correction. Additionally, the following corrections described in the supplement of Baryshnikova et al. (2010), were disabled due to biological or technological differences between *C. neoformans* chemical genomics and *S. cerevisiae* genetic interactions: genetic linkage filter, large colony filter, and jackknife variance filter. Ten replicates of the glucose condition served as the wild-type control. Any strain which did not have data for at least 65% of the tested conditions after all corrections and filters was removed from analysis. Multiple replicates ($n \geq 7$) were run for MMS (a low-variance small molecule condition) and rapamycin (a high-variance small-molecule condition) to provide estimates of within-small molecule condition variance.

C. neoformans Ortholog Identification and GO Term Mapping

Mapping from *S. cerevisiae* Uniprot Proteins to *C. neoformans* Uniprot Proteins was done using One-to-one mappings in MetaPhOrs (http://metaphors.phylomedb.org/). *C. neoformans* ORFs were blasted against a database of *S. cerevisiae* Uniprot Proteins using blastp (Altschul et al., 1997) with a E-score cutoff of 10^{-30}. The corresponding yeast GO annotations were mapped onto the *C. neoformans* ORFs.

We then calculated whether small molecules that elicited a sensitive phenotype from *C. neoformans* knockout mutants targeted mutants of ORFs enriched for specific GO terms. First, we filtered out any small-molecule profile that did not have at least a pairwise 0.3 cosine correlation for all pairs of the same small molecule and those for which we only had a single concentration of a small molecule. GO terms with ≤ 3 associated *C. neoformans* ORFs were also removed from analysis. We then averaged data from the same small molecule at different concentrations to form a single "chemical-genetic profile" for each small molecule. Any individual chemical-genetic interaction score within a profile that was less than the first percentile or greater than the 99th percentile was set to the first or 99th percentile, respectively. We used a Z-score cutoff of < -2.5 to identify significant "sensitive" phenotypes. Enrichment was calculated by determining the mean chemical-genetic score for each separate small-molecule treatment for all knockout mutants whose ORF belong to a specific GO term. We then calculated how extreme that mean was relative to the chemical-genetic score for all knockout mutants when treated with that small molecule. A p value ≤ 0.05 was considered significant. 20 randomizations were done by permuting the gene labels of small-molecule-gene interaction datapoints, which we used to estimate false discovery rate (FDR) of 0.17. All analyses in Figures 2 and 3 were also performed on randomized, label-swapped data and only datapoints enriched relative to the randomized data (p value ≤ 0.05) is shown.

Comparison of *C. neoformans* and *S. cerevisiae* Transcriptional Responses to Fluconazole

A list of genes with transcriptional changes in response to fluconazole in *C. neoformans* was retrieved from Florio et al. (Florio et al., 2011) and a comparable list for *Saccharomyces cerevisiae* was retrieved from Kuo et al. (Kuo et al., 2010). We note that the Kuo et al. study identified significantly more differentially expressed genes (~1,300 as compared to ~170), likely due to more extensive sampling of the response across time and a greater number of replicates. Kuo et al. grouped these ~1,300 genes into 17 different clusters, so we assessed each cluster as well as the entire set for its overlap with the *Cryptococcus* orthologs (Table S7). A hypergeometric test was performed to assess the significance of each overlap. Globally, we observed a significant overlap between the two species (56 of the 170 *Cryptococcus*-responsive genes overlapped with the *S. cerevisiae* response, p value = 1.59×10^{-3}). When each *S. cerevisiae* cluster was evaluated independently, we observed a significant overlap for 4 out of 17 clusters of differentially expressed genes (p value < 0.05). Note that although this overlap is statistically significant, there is a substantial difference in the transcriptional

response between the two species. For example, 114 of the 170 (~67%) *Cryptococcus*-responsive genes were not observed as differentially expressed in *S. cerevisiae* despite the sensitivity of the *S. cerevisiae* study.

Knockout Strain Construction

Strain construction was performed as previously described (Liu et al., 2008).

Capsule Induction Assay

Samples were grown overnight at 30°C in 100% Sabouraud's broth, then diluted 1:100 into 10% Sabouraud's broth buffered with 50 mM HEPES pH 7.3 and grown for 3 days at 37°C. India ink was added at 3:1 ratio and samples imaged on a Zeiss Axiovert microscope. Capsule + cell and cell alone diameters were determined using Zeiss axiovision software.

Capsule Transfer Assay

These assays were performed as in (Reese and Doering, 2003), with minor modifications. Briefly, GXM donor strains were grown 6 days at 30°C in 1× YNB with shaking. Cultures were centrifuged to remove cells, then supernatants passed through a 0.22?m filter to make conditioned medium. An acceptor *cap59*Δ strain was grown overnight in YNB, washed twice in 1× PBS, then resuspended at a final concentration of 2.5×10^6 cells/ml. 2 μl of 1:10 conditioned medium was added to 2.5×10^5 cells (100 μl) (final concentration conditioned medium 1:500), then samples incubated for 1 hr with rotation at room temperature (RT). Samples were washed twice in 1× PBS, resuspended in 50 μl 1× PBS + 1% bovine serum albumin (BSA) + 1:100 anti-GXM antibody (mAb 339), the incubated 1 hr at RT with rotation. 1:200 anti-mouse TRITC was added, samples incubated 1 hr at RT with rotation, then imaged on a Zeiss Axiovert microscope.

GXM Immunoblot

Conditioned medium was made from donor GXM donor strains as described above. 5 μl conditioned medium per donor strain was run on a 0.6% 1× TBE agarose gel. Samples were transferred to a positively charged nylon membrane by blotting overnight using standard procedures for Southern blots. The membrane was then dried, blocked 1 hr in 1× TBS + 0.1% Tween-20 + 5% milk. Membrane was then incubated overnight at 4°C in 1× TBS + 5% milk + 1:1,000 anti-GXM MAb339, washed twice in TBS, incubated 2 hr in TBS + 5% milk + 1:2,000 anti-mouse HRP-conjugated antibody, washed 2 hr in TBS + 0.1% Tween-20, then developed.

Mouse Infection Assay

Mouse lung infections were performed as previously described (Chun et al., 2011).

Cdc25 Protein Purification

We identified the *C. neoformans* ortholog of Cdc25, *CNAG_01572*, by best reciprocal BLAST (Altschul et al., 1997) hit with the human Cdc25A, Cdc25B, and Cdc25C protein isoforms. The exonic sequence of the catalytic domain of the *C. neoformans* ortholog of Cdc25, *CNAG_01572* (aa442-662), was synthesized and cloned into the pRSET A vector by Biomatik. Following transformation into BL21 *E. coli* cells, we grew cultures overnight at 30°C in 2× LB + 100 μg/ml carbenicillin. 5 ml overnight cultures were used to inoculate two flasks of 500 ml 2× LB + carbenicillin, which were then grown at 30°C for 3 hr. We then transferred the cultures to 20°C and added IPTG to 1 mM to induce protein expression. Cells were then harvested and lysed using B-PER bacterial protein extraction reagent (Thermo Scientific) according to the manufacturer's instructions. Cell extracts were run over a 22 ml capacity centrifugation columns packed with 3 ml HisPur Cobalt Resin (Thermo Scientific). Columns were packed and prepared according to the manufacturer's instructions. Cell extracts were mixed with 2 volumes equilibration/wash buffer (50 mM sodium phosphate, 300 mM sodium chloride, 5 mM imidazole, 1× EDTA-free protease inhibitors [Roche], pH 7.4), equilibrated 30 min at 4°C with rotation, centrifuged 2 min at 700 × *g*, then washed three times in two resin-bed volumes (6 ml) of equilibration/wash buffer. Protein was then eluted three times in 3 ml elution buffer (50 mM sodium phosphate, 300 mM NaCl, 150 mM imidazole, 1× EDTA-free protease inhibitors, pH 7.4). Eluates were analyzed by Coomassie staining, assayed for phosphatase activity, and pure fractions with activity were pooled for downstream analysis.

Cdc25 Phosphatase Assay

Cdc25 phosphatase activity was analyzed in activity buffer (50 mM Tris pH 8.3, 5% glycerol, 0.8 mM dithiolthreitol, and 1% PVA). Reactions were prepared from 5× activity buffer stock; 1:10 dilution of purified *C. neoformans* Cdc25 protein; NA8, S8, or S10 inhibitors at variable concentrations; and 3-O-methylfluorescein phosphate substrate (Sigma-Aldrich, M2629) at 5–30 μM final concentration. Assays were run on a Tecan Infinite 200 plate reader, excitation wavelength 485 nm, emission wavelength 525 nm, reading every 2.5 min for 20 min. Kinetics were calculated using GraphPad Prism.

Cdc25 Inhibitor Treatment and FACS Analysis

Wild-type *C. neoformans* was grown overnight in 1× YNB at 30°C with rotation. Cultures were diluted to OD_{600} ~0.2 into 150 ml 1× YNB, then incubated 3 hr at 30°C. Samples were then split and NA8, S8, and S10 added to 60 μM. Equivalent volume of DMSO was added to the control culture; 1 ml samples were harvested every 30 min and resuspended in 1 ml 70% EtOH and fixed overnight at

4°C. Samples were resuspended to ~10^7 cells/ml, washed 1× in 50 mM sodium citrate (pH 7.0), briefly sonicated, then incubated with 250 μg/ml RNase A at 50°C for 1 hr, followed by 1 mg/ml proteinase K for 1 hr at 50°C. 0.5 ml sample was added to 50 mM sodium citrate + 16 μg/ml propidium iodide, then incubated overnight at 4°C. Samples were lightly sonicated before analysis on FACSCaliburDxP8 (B.D. Biosciences).

Fractional Inhibitory Concentration Index Assay for Small Molecule Synergy

We determined FICI using a standard checkerboard assay (Hsieh et al., 1993), calculating FICI as described using a 50% growth inhibition cutoff for MICs for individual small molecules (Hsieh et al., 1993; Meletiadis et al., 2010), then using a standard cutoff of FICI < 0.5 to define synergy. Checkerboard plates were inoculated from an overnight wild-type *C. neoformans* culture that was washed twice in 1× PBS. Final concentration was OD_{600} ~0.1. OD_{600} for each 96-well plate was read in a Tecan Infinite 200 plate reader at 0 hr, 24 hr, and 48 hr postinoculation. Plates were incubated at 30°C prior to measurement.

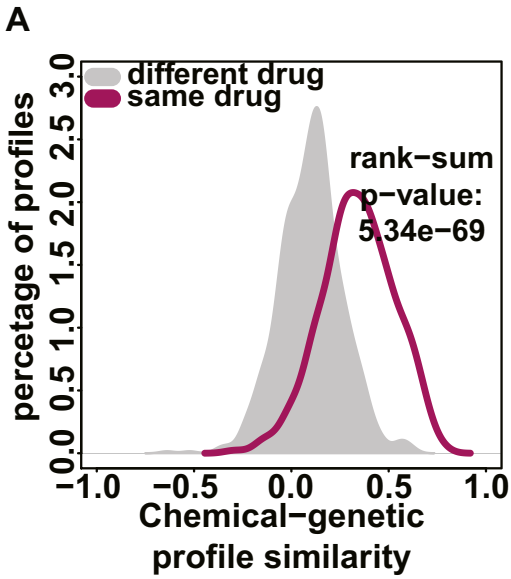

Figure S1. Data Normalization, Related to Figure 1

Pairwise correlation scores (cosine similarity) between the chemical genetic profiles of different compounds (gray) and the same compounds at different concentrations (purple) screened on same day (same batch). Pairwise correlation scores of similar value were binned together (x axis) shown relative to the percentage of the total population (y axis). Correlation scores between the chemical-genetic profiles of the same compounds are significantly higher than those between different compounds (Wilcoxon test, $p = 5.3 \times 10^{-69}$).

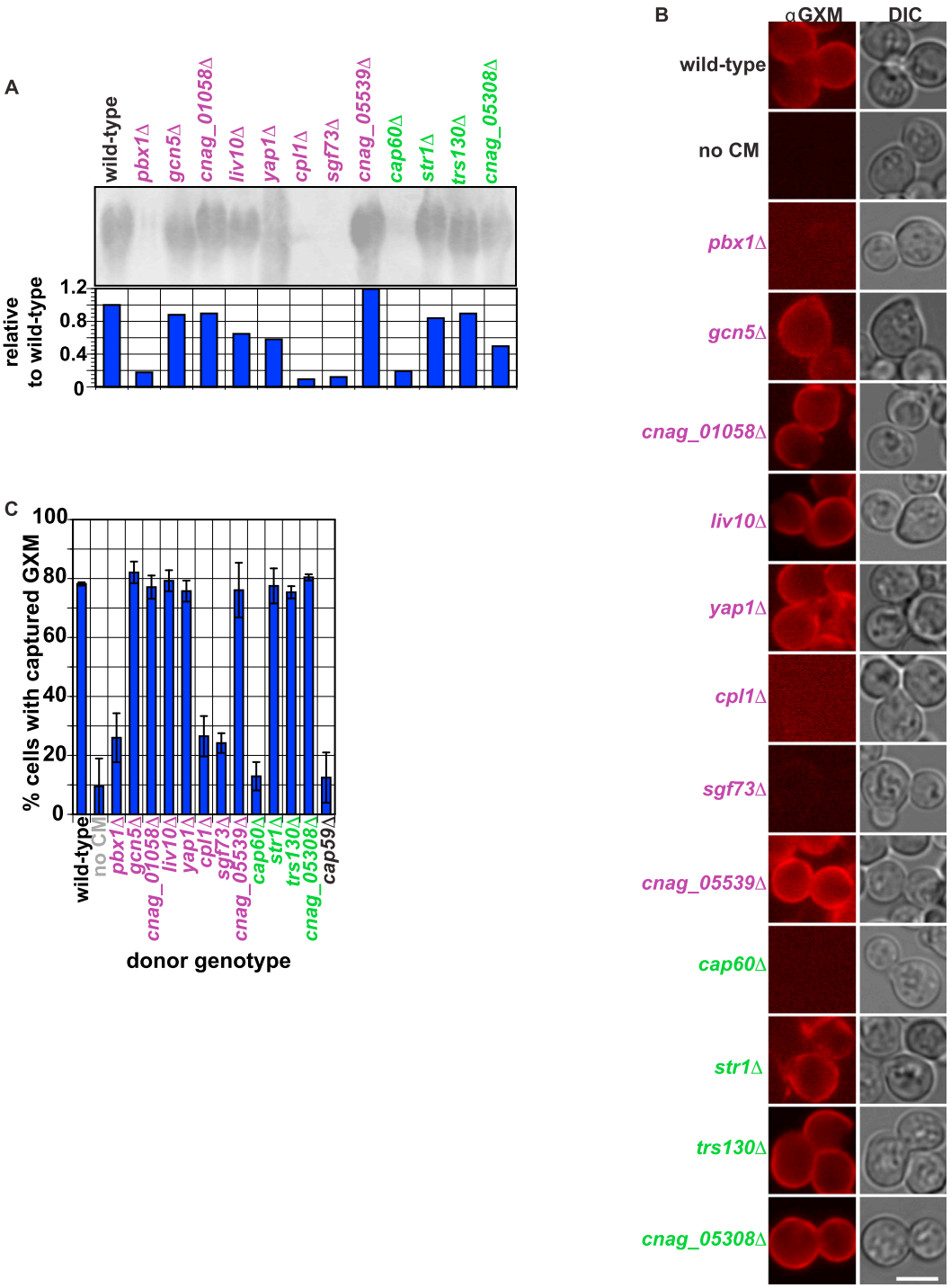

Figure S2. *PBX1* Cluster Genes Are Involved in Maintenance of GXM on the Cell Surface, Related to Figure 4

(A) Blot against GXM from conditioned medium. Cells were grown for one week to produce conditioned medium.

(B) Representative images from capsule transfer assay. Scale bar, 5 μm.

(C) Quantification of capsule transfer assay. 200 cells were counted for each experiment. Columns show the average of three experiments and error bars represent the standard deviation. Asterisk represents p value of 0.007 or lower (Student's t test).

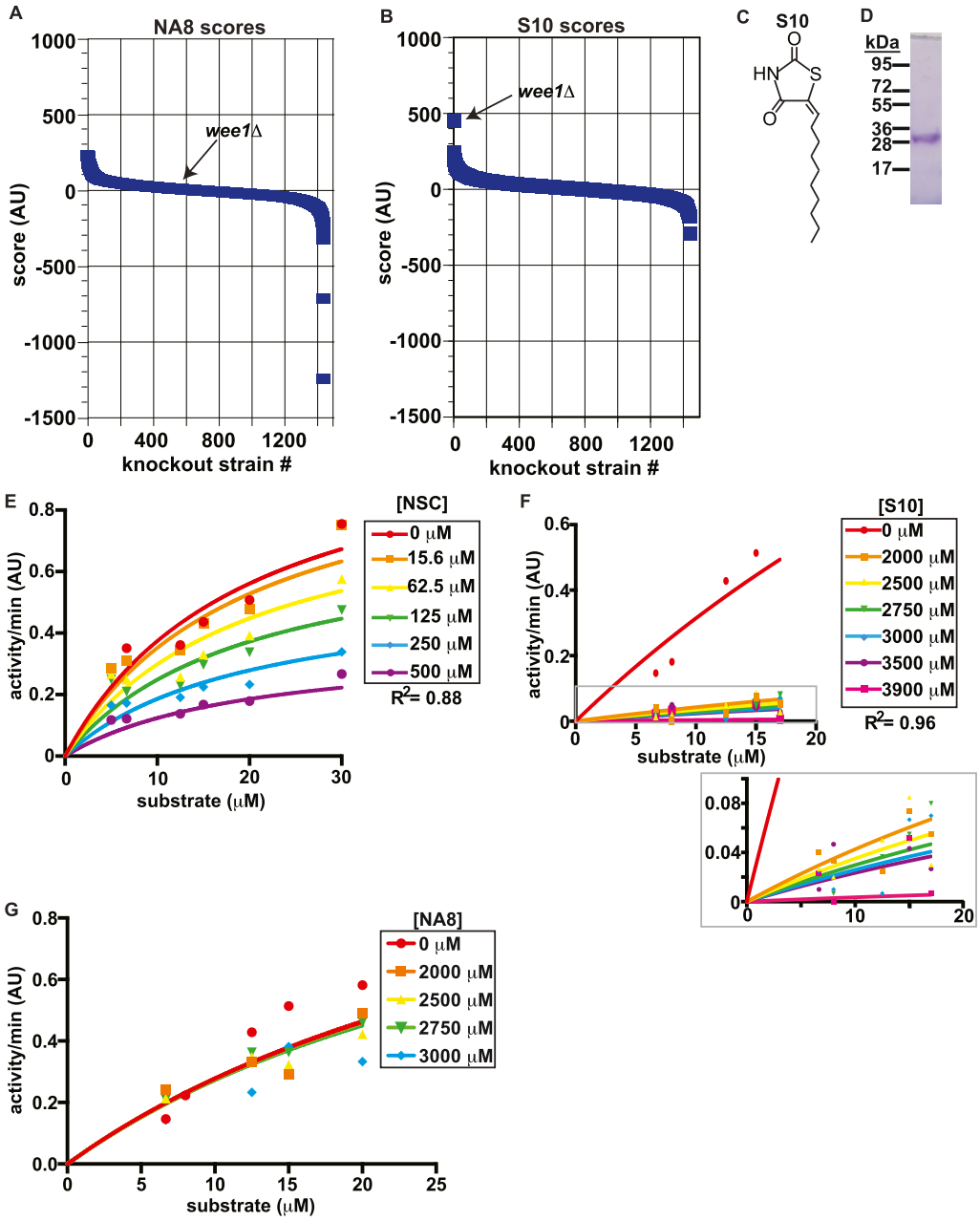

Figure S3. S10 Targets *C. neoformans* Cdc25, Related to Figure 5

(A) Chemical-genetic data of the growth scores of each knockout mutant grown on NA8 (y axis). Unlike S8, *wee1*Δ did not exhibit significant resistance.

(B) Chemical-genetic data of the growth scores of each knockout mutant grown on S10 (y axis). As with S8, the mutant that exhibited the greatest resistance is *wee1*Δ. C: S10 structure.

(C) Structure of S10.

(D) Purified *C. neoformans* Cdc25 protein.

(E) Michaelis-Menten kinetics of S10 inhibition of *Cn*Cdc25 from in vitro phosphatase activity. A noncompetitive (allosteric) model of enzyme inhibition produced the best R^2 value (0.96). Grey box is shown in inset.

(F) Michaelis-Menten kinetics of NSC 663284 inhibition of *Cn*Cdc25 from in vitro phosphatase activity. A noncompetitive (allosteric) model of enzyme inhibition produced the best R^2 value (0.88).

(G) Michaelis-Menten kinetics of *Cn*Cdc25 in vitro phosphatase activity NA8 inhibition of *Cn*Cdc25 from in vitro phosphatase activity. NA8 does not detectably inhibit *Cn*Cdc25.